Adaptive mesh refinements for thin shells whose middle surface is not exactly known

Ph. Destuynder [a], Y. Moguen [b,*], M. Salaün [c]

[a] Conservatoire National des Arts et Métiers, Chaire de Calcul Scientifique, 292 rue Saint-Martin, F-75141 Paris Cedex 03, France
[b] Université de Pau et des Pays de l'Adour, Laboratoire de Thermique, Energétique et Procédés, IUT GTE, 1 avenue de l'Université, F-64000 Pau, France
[c] Université de Toulouse, ISAE, 10 avenue E. Belin, F-31055 Toulouse, France

A B S T R A C T

A strategy concerning mesh refinements for thin shells computation is presented. The geometry of the shell is given only by the reduced information consisting in nodes and normals on its middle surface corresponding to a coarse mesh. The new point is that the mesh refinements are defined from several criteria, including the transverse shear forces which do not appear in the mechanical energy of the applied shell formulation. Another important point is to be able to construct the unknown middle surface at each step of the refinement. For this, an interpolation method by edges, coupled with a triangle bisection algorithm, is applied. This strategy is illustrated on various geometries and mechanical problems.

Keywords:
Shell
Adaptive mesh refinement
Geometry approximation
Mixed finite elements method
A posteriori error estimation

1. Introduction

The problem of adaptive mesh refinements on shells remains a seldom studied subject. Compared with more classical models like plates or bidimensional elasticity problems, one has to deal with an additional difficulty which is that the mesh to refine is not plane. For instance, the center of mass of a triangle or of a quadrangle is generally not on the middle surface of the shell even if the nodes are on it. It is the reason why it is often assumed that the exact shell geometry is known, analytically or from a computer aided design program. For example, in [1–4], the exact mapping defining the shell geometry is supposed to be known and a completely new mesh, based on spatial distribution of new element sizes, is defined at each step of the refinement procedure. In another way, it is suggested in [5] to create a new mesh by moving the vertices of the previous one, while isogeometric formulations used in [6], assumes that the geometry is exactly known from NURBS. This enables one to construct a mesh of "NURBS elements", which is easy to refine by reindexation of the parametric space. Despite their interest, these two approaches also need the knowledge of the exact geometry of the shell surface. Finally, in the case of shell structures, [7] is one of the very few papers in which the initial mesh is the basis of the next one, in the sense that some of its elements are divided in order to obtain the new mesh. But again, these authors assume that the exact shell geometry is known. In fact, they introduce in their numerical experiments the idea of quality of the geometry approximation as a refinement criteria. This one is expressed as a function of the errors on the added nodes position and the unit normal vectors at these points.

In this paper, a new approach is suggested. A refinement strategy is introduced in association with an approximation of the middle surface of the shell. It is only assumed that (1) the positions of the vertices of a set of flat triangular elements approximating the middle surface and (2) the normal vectors at these vertices, are known from a coarse mesh of the middle surface of the shell. Then, following a methodology developed in [8], it is possible to build new vertices for each element which are closer to the middle surface than the middle of the element edges.

Concerning the choice of the refinement criteria, let us make few remarks. The usual estimators, such as those of Zhu and Zienkiewicz (see [9,10]) for example, are appropriate for a global error control. Nevertheless, in some papers (see for example [11,12]), the concept of variable of interest is introduced in the definition of the error indicator. In the case of thin structures, such as plates and shells, transverse shear forces are such obvious quantities of interest. By the way, among Kirchhoff–Love assumptions, one is the nullity of the transverse shear strains (but not the shear forces). Moreover, the transverse shear forces are considered as neglectible in front of the inplane stresses in the constitutive relationship. But, it is precisely the stress component which is necessary in order to satisfy the three-dimensional equilibrium equation through the

* Corresponding author. Tel.: +33 5 59 40 71 59; fax: +33 5 59 40 71 60.
E-mail address: yann.moguen@free.fr (Y. Moguen).

thickness of the shell. So, it can be pointwise very different from zero (it can be a mathematical measure). Obviously, this phenomenon should be taken into account in the refinement criteria. It is the basic point in the definition of the error indicator described hereafter.

The plan of this paper is the following one. In Section 2, few notations related to shells are introduced. The finite element formulation used is described in Section 3, while Section 4 concerns the mesh refinement strategy. In Section 5, the mesh refinement criteria is introduced and, finally, various numerical examples are presented in the last section.

2. Geometrical aspects for shells

Let us recall that a shell is a three-dimensional structure for which one dimension, called the thickness, is very small compared to the other dimensions (maximum length or local radius of curvature). In this paper, the middle surface of the shell will be denoted by ω while half the thickness will be ε. Finally, as a shell formulation is used, even if it is a mixed one, let us introduce now some basic elements of differential geometry. For more details see [13], for example.

So, it is assumed that there exists a mapping, say ϕ, from an open set $\hat{\omega}$ onto the middle surface ω which is at least $\mathscr{C}^3(\hat{\omega})$. The plane $\mathbb{R}^2$ containing $\hat{\omega}$ will be referred to coordinates (ξ^1,ξ^2) while the space $\mathbb{R}^3$ is referred to an orthonormal system of coordinates $(O;e_1,e_2,e_3)$. Then, one has

$$\omega=\{m\in\mathbb{R}^3 \mid m=\phi(\xi^1,\xi^2),(\xi^1,\xi^2)\in\hat{\omega}\}.$$

Corresponding to the mapping ϕ, a curvilinear system of coordinates is defined on ω such that, at any point $m=\phi(\xi^1,\xi^2)$ of ω, the tangent vectors are (see Fig. 1)

$$a_1=\phi_{,1}\equiv\frac{\partial\phi}{\partial\xi^1},\quad a_2=\phi_{,2}\equiv\frac{\partial\phi}{\partial\xi^2}.$$

Let us assume that the vectors a_1 and a_2 are linearly independent and span the tangent plane at each point m of ω. The unit normal vector at point m is then defined by

$$N=\frac{a_1\wedge a_2}{\|a_1\wedge a_2\|}.$$

For the sake of brevity, in the following, Greek indices are assumed to belong to the set $\{1,2\}$ and the implicit summation convention over repeated indices is adopted.

Let us now define several quantities, which are necessary for the definition of the shell model. The first fundamental form on surface ω is given by

$$g_{\alpha\beta}=a_\alpha\cdot a_\beta, \tag{1}$$

where "·" stands for the euclidian scalar product. This tensor is also called the metric tensor. Its determinant is $|g|=g_{11}g_{22}-g_{12}^2$ and its inverse is such that

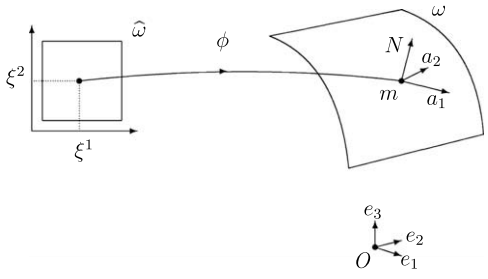

Fig. 1. Definition of surface ω.

$$g^{\alpha\beta}=a^\alpha\cdot a^\beta, \tag{2}$$

where $\{a^\alpha\}$, called the dual basis of $\{a_\alpha\}$, is defined with the vectors a^α such that: $a^\alpha\cdot a_\beta=\delta^\alpha_\beta$ (Kronecker's symbol). Then, let us introduce $a_{\alpha,\beta}$, which is the partial derivative of a_α with respect to ξ^β. One can write this vector in the basis (a_1,a_2,N) and obtain $a_{\alpha,\beta}=\Gamma^\gamma_{\alpha\beta}a_\gamma+b_{\alpha\beta}N$, where $\Gamma^\gamma_{\alpha\beta}$ are the Christoffel's symbols. $b_{\alpha\beta}$ is the second fundamental form on ω, also called the curvature. One has

$$b_{\alpha\beta}=N\cdot a_{\alpha,\beta},\quad \Gamma^\gamma_{\alpha\beta}=a^\gamma\cdot a_{\alpha,\beta}. \tag{3}$$

3. A mixed variational formulation for the Koiter's shell model

3.1. The Koiter's shell model

The Koiter's shell model is used (see [14,15]). It is formulated using the two following strain tensors. The first one represents the change of metric on the surface ω due to a displacement. It is denoted by $\gamma_{\alpha\beta}$. The second one, named $\rho_{\alpha\beta}$, is the change of curvature suggested by Budiansky and Sanders [15]. If v is a displacement vector field on the surface ω, expressed in local coordinates by $v=v^\alpha a_\alpha+v_3N$, then $\gamma_{\alpha\beta}(v)$ and $\rho_{\alpha\beta}(v)$ are, respectively, given by

$$\begin{cases}\gamma_{\alpha\beta}(v)=\frac{1}{2}(v_{\alpha|\beta}+v_{\beta|\alpha})-b_{\alpha\beta}v_3,\\ \rho_{\alpha\beta}(v)=\frac{1}{2}(\theta_{\alpha|\beta}+\theta_{\beta|\alpha})+\frac{1}{2}(b^\lambda_\alpha v_{\beta|\lambda}+b^\lambda_\beta v_{\alpha|\lambda})-b^\lambda_\alpha b_{\lambda\beta}v_3\end{cases} \tag{4}$$

with $b^\lambda_\alpha=g^{\lambda\beta}b_{\beta\alpha}$ and $v_{\alpha|\beta}=v_{\alpha,\beta}-\Gamma^\gamma_{\alpha\beta}v_\lambda$ (covariant derivative). Finally, the transverse section rotations θ_α can be expressed through the Kirchhoff–Love kinematical relation by

$$\theta_\alpha=-b^\lambda_\alpha v_\lambda-v_{3,\alpha}. \tag{5}$$

An important point to be noticed is that the expression of $\rho_{\alpha\beta}(v)$ requires the derivatives of θ_α, then those of b^λ_α. As b^λ_α depends on the second derivatives of the mapping ϕ (see (3)), such a model needs the third derivatives of ϕ.

Hence, the classical shell model consists in finding a displacement field u belonging to the set V of the admissible displacement fields, and such that for all $v\in V$,

$$\int_\omega R^{M\alpha\beta\lambda\mu}\gamma_{\alpha\beta}(u)\gamma_{\lambda\mu}(v)+\frac{\varepsilon^2}{3}\int_\omega R^{F\alpha\beta\lambda\mu}\rho_{\alpha\beta}(u)\rho_{\lambda\mu}(v)=l(v), \tag{6}$$

where $R^{M\alpha\beta\lambda\mu}$ and $R^{F\alpha\beta\lambda\mu}$ are, respectively, the membrane and the bending stiffness tensors. In the particular case of an homogeneous and isotropic material,

$$R^{M\alpha\beta\lambda\mu}=R^{F\alpha\beta\lambda\mu}=\frac{E\varepsilon}{1-\nu^2}((1-\nu)(g^{\alpha\lambda}g^{\beta\mu}+g^{\alpha\mu}g^{\beta\lambda})+2\nu g^{\lambda\mu}g^{\alpha\beta}),$$

where E is the Young's modulus and ν the Poisson's ratio. Finally, $l(v)$ stands for the mechanical loading.

3.2. Continuous mixed variational formulation

The main ideas of the mixed formulation, introduced in [16], are the following. First of all, the transverse section rotations θ_α are

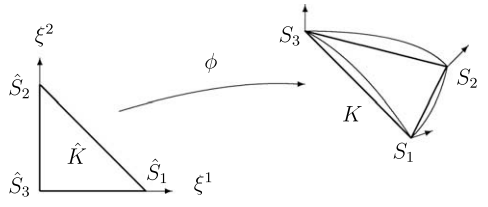

Fig. 2. Approximation of the middle surface geometry.

introduced as new unknowns. This is very usual in plate and shell theories. Second, the Kirchhoff–Love relationship (5) is prescribed by means of a Lagrange multiplier. Let us observe that this multiplier has the physical meaning of the resultant transverse shear forces vector, which will be useful for the definition of refinement criteria.

Let us now be more precise. We introduce the membrane forces tensor $n^{\alpha\beta} = R^{M\alpha\beta\lambda\mu}\gamma_{\lambda\mu}(u)$, the bending moments tensor $m^{\alpha\beta} = R^{F\alpha\beta\lambda\mu}\rho_{\lambda\mu}(u)$, where $\gamma_{\lambda\mu}(u)$ and $\rho_{\lambda\mu}(u)$ are given in (4), and the resultant transverse shear forces vector, say $q = q^{\alpha}a_{\alpha}$. The basic point of the method is to split q into the sum of the gradient of a scalar function and the rotational of another one (Helmholtz decomposition), like

$$q = \operatorname{grad}\varphi + \operatorname{rot}\psi = g^{\alpha\beta}\varphi_{,\beta}a_{\alpha} + \frac{1}{\sqrt{|g|}}(-\psi_{,2}a_1 + \psi_{,1}a_2). \tag{7}$$

So, starting from the equilibrium relationships and writing (7) in a variational form, the global mixed formulation reads

$$\begin{cases} \text{find } (\Lambda, X) \in \mathscr{M} \times \mathscr{V} \text{ such that} \\ \forall Y \in \mathscr{V}, \quad A(X,Y) + B(\Lambda, Y) = L(Y), \\ \forall \Xi \in \mathscr{M}, \quad B(\Xi, X) = 0, \end{cases} \tag{8}$$

where the unknowns are $X = (u_{\alpha}, u_3, \theta_{\alpha})$ and $\Lambda = (\varphi, \psi)$ associated with the virtual fields $Y = (v_{\alpha}, v_3, \mu_{\alpha})$ and Ξ. Let us remark that, from now on, u_{α}, u_3 and θ_{α} are considered as independent variables. Moreover, $L(Y)$ is the natural extension of the linear form $l(v)$ appearing in (6). The bilinear form A reads

$$\begin{aligned} A(X,Y) &= \int_{\omega} R^{M\alpha\beta\lambda\mu}\gamma_{\alpha\beta}(X)\gamma_{\lambda\mu}(Y) + \frac{\varepsilon^2}{3}\int_{\omega} R^{F\alpha\beta\lambda\mu}\rho_{\alpha\beta}(X)\rho_{\lambda\mu}(Y) \\ &= \int_{\omega} n^{\alpha\beta}(X)\gamma_{\alpha\beta}(Y) + \frac{\varepsilon^2}{3}\int_{\omega} m^{\alpha\beta}(X)\rho_{\alpha\beta}(Y) \end{aligned} \tag{9}$$

and gives the elastic energy of the shell while B, expressed by

$$\begin{aligned} B(\Lambda, Y) = \frac{\varepsilon^2}{3}\Bigg[&\int_{\omega} g^{\alpha\lambda}\varphi_{,\lambda}(\mu_{\alpha} + b_{\alpha}^{\beta}v_{\beta} + v_{3,\alpha}) \\ &- \int_{\omega} \frac{\psi}{\sqrt{|g|}}(\mu_{2,1} - \mu_{1,2} + (b_2^{\beta}v_{\beta})_{,1} - (b_1^{\beta}v_{\beta})_{,2})\Bigg], \end{aligned} \tag{10}$$

ensures the Kirchhoff–Love constraint (5). As a matter of fact, displacement fields X such that $B(\Xi, X) = 0$ for all $\Xi \in \mathscr{M}$, are precisely Kirchhoff–Love displacement fields. Finally, the functional spaces are defined by

$$\mathscr{V} = V_t \times V \times W_t, \quad \mathscr{M} = V \times L_0^2(\omega)$$

with

$$\begin{cases} V_t &= \{v_t = v^{\alpha}a_{\alpha} \mid v^{\alpha} \in H^1(\omega); v^{\alpha} = 0 \text{ on } \gamma_0 \cup \gamma_1\}, \\ V &= \{v \in H^1(\omega) \mid v = 0 \text{ on } \gamma_0 \cup \gamma_1\}, \\ L_0^2(\omega) &= \{\psi \in L^2(\omega) \mid \int_{\omega}\psi = 0\}, \\ W_t &= \{\mu = \mu_{\alpha}a^{\alpha} \mid \mu_{\alpha} \in H^1(\omega); \mu_{\alpha} = 0 \text{ on } \gamma_0; \mu_t = 0 \text{ on } \gamma_1\}, \end{cases}$$

where μ_t stands for the tangential component along the edge. Moreover, to make the boundary conditions more precise, γ_0 and γ_1 are two parts of the boundary γ of ω, where the shell is assumed to be clamped and simply supported, respectively. The remainder of the boundary of ω is free.

To conclude this section, let us emphasize an advantage of this formulation. We have observed that the classical variational formulation needs the use of the third-order derivatives of the mapping ϕ describing ω. Here, these derivatives should appear in the bilinear form B. But a simple calculus leads to the relation

$$(b_2^{\beta}v_{\beta})_{,1} - (b_1^{\beta}v_{\beta})_{,2} = b_2^{\beta}v_{\beta,1} - b_1^{\beta}v_{\beta,2} + (\Gamma_{\mu 2}^{\beta}b_1^{\mu} - \Gamma_{\mu 1}^{\beta}b_2^{\mu})v_{\beta},$$

and the third-order derivatives disappear. This point will be of importance when the geometry of the shell is not exactly known and an approximation of it has to be constructed.

3.3. Numerical discretization

In the case of classical variational formulations, such as (6), the main condition, which ensures existence and uniqueness of a solution, is the ellipticity of the bilinear form. So, when a conformal finite element approximation is used, which means that the discrete space is contained in the continuous one, this ellipticity property is kept and the discrete model has also one and only one solution (see [17]). Unfortunately, this condition of conformity of the discrete spaces is not sufficient in the case of mixed formulations. This

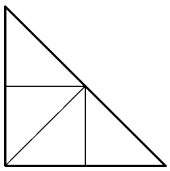

Fig. 3. First refinement of a triangle.

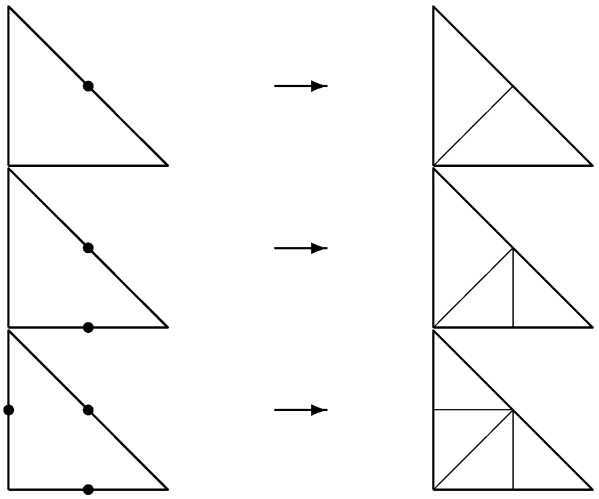

Fig. 4. Next refinements of a triangle to obtain conformity.

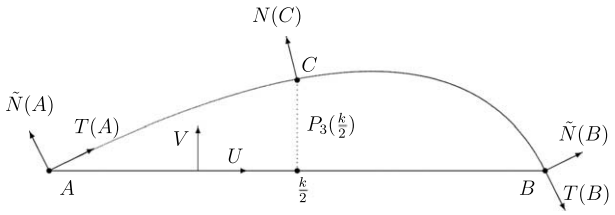

Fig. 5. Approximation of the middle surface in the plane Π.

Table 1
Settings for the cylinder under uniform pressure and the cracked cylindrical shell

Length	Thickness	Radius	Young's modulus	Poisson's ratio	Pressure
$L = 100$	$2\varepsilon = 1$	$R = 100$	$E = 3 \times 10^9$	$\nu = 0.3$	$P = 3 \times 10^5$

problem is well-known in fluid mechanics and is due to the incompressibility condition. A long time ago (for example, see [18]), efficient numerical schemes were suggested to overcome this difficulty. In this case, where the main unknowns are velocity and pressure, the idea is to enrich the velocity. We follow this idea, keeping in mind that the field which takes the place of velocity is the transverse section rotations θ_α vector.

Practically, first-order degree polynomials are used for each unknown $u_\alpha, u_3, \theta_\alpha, \varphi$ and ψ. But, in order to stabilize the numerical scheme, the rotations θ_α are enriched with internal degrees of freedom. More precisely, if triangular elements are used, which is the case in the following of this paper, a "bubble" function is added for each rotation θ_α. With this scheme, it can be proved that the error estimate between the exact solution and the discrete one is of order $\mathcal{O}(h)$, if h stands for the small parameter linked to the mesh size (see [19]).

4. Approximation of the middle surface of the shell and refinement strategy

4.1. Approximation of the middle surface

Now, it is assumed that the middle surface ω of the shell is approximated by flat triangular elements, the vertices of which

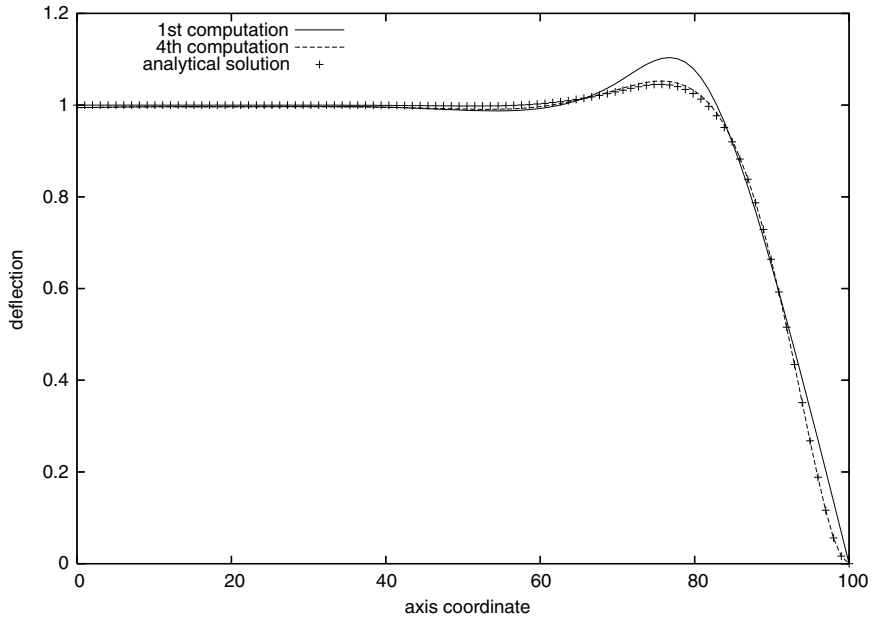

Fig. 6. Cylinder under uniform pressure ($\alpha = 0.25$) – deflection along the axis direction.

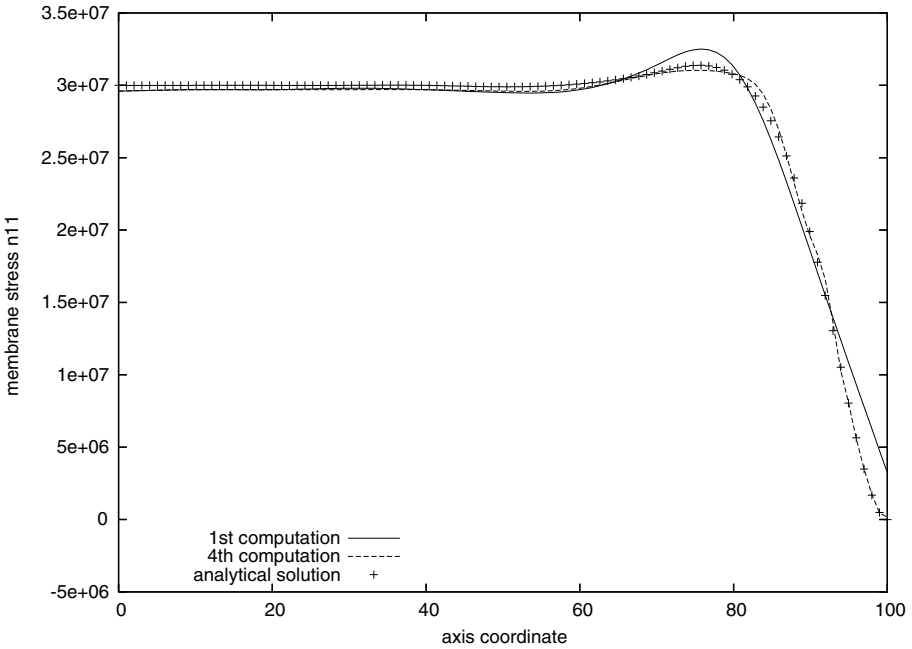

Fig. 7. Cylinder under uniform pressure ($\alpha = 0.25$) – membrane force n_1^1 along the axis direction.

are on ω. Moreover, it is assumed that the normal vectors to ω at these vertices are exactly known (see Fig. 2). Then, it is possible to build a local basis, *i.e.* depending on the element, of the tangent plane at each vertex of the mesh. From an interpolation of these "nodal" bases, one can obtain an approximation of the geometrical tensors (1)–(3), which are needed in the shell model. And it can be proved that the error, due to this approximation, is also of order $\mathcal{O}(h)$ in energy norm, which is the same as the error due to the finite element interpolation (see [20]).

4.2. Mesh refinement: basic aspects

Let us begin with the technical aspects of the mesh refinement, recalling that we use meshes only made of triangles. In order to refine these meshes, an algorithm proposed by Rivara is used (see [21]). Its main ideas are the following ones. In a first time, each triangle which has to be refined, is divided into four sub-triangles, in the following manner (see Fig. 3): the middle point of the longest

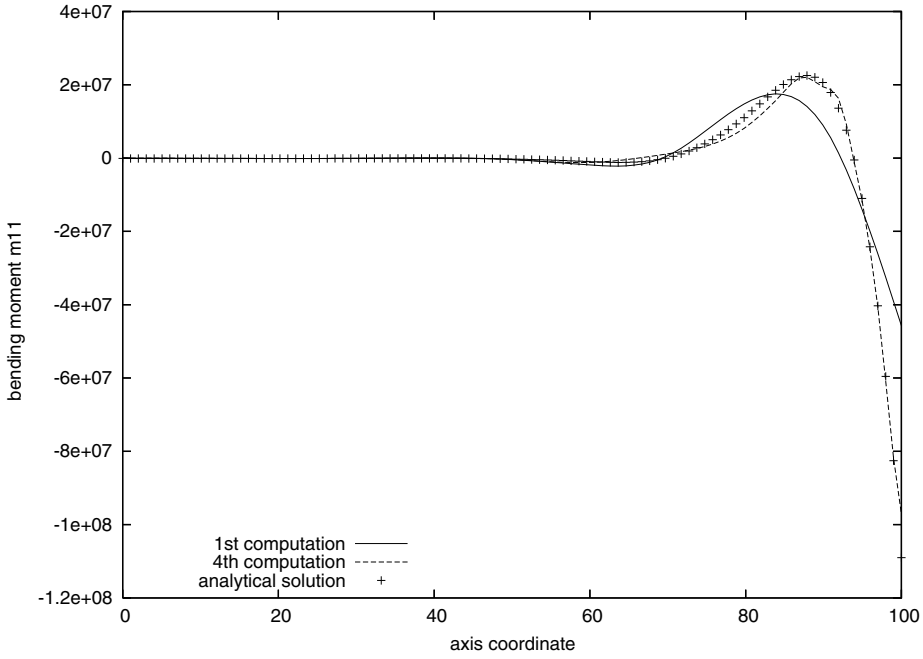

Fig. 8. Cylinder under uniform pressure ($\alpha = 0.25$) – bending moment m_1^1 along the axis direction.

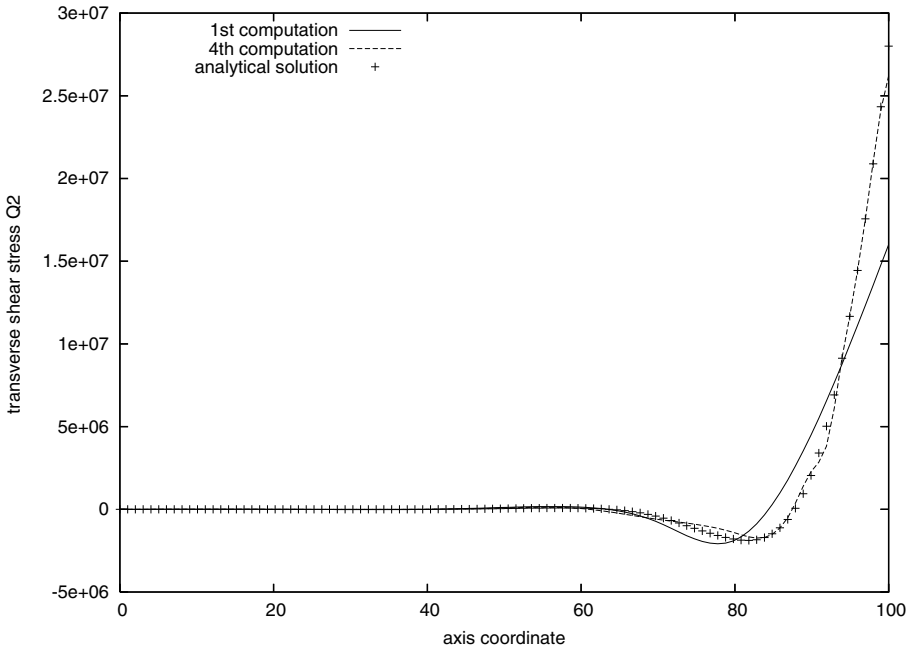

Fig. 9. Cylinder under uniform pressure ($\alpha = 0.25$) – transverse shear force q^2 along the axis direction.

side is connected with its opposite vertex and with the middle points of the two other sides.

Once this first refinement is achieved, a second one is done to ensure the conformity of the new mesh. So, two cases may occur. If a new node is added on the longest side of a triangle, it is connected with it opposite vertex. If not, it is connected with the middle point of the triangle longest side (see Fig. 4). This process is repeated until total conformity is obtained, which practically occurs after a few iterations. Finally, let us emphasize a major advantage of this technique: during the successive refinements, the final mesh has angles which remain bounded away from zero (see [21]).

4.3. Mesh refinement: case of shell structures

As far as refinement is concerned, we have to deal now with the fact that the mesh to refine is not plane. Thus, the middle point of a triangle edge is generally not on the surface. So, we shall use a methodology developed by one of the authors and a coworker (see [8]). For autonomy of this paper, let us describe this strategy hereafter.

Let A and B be two vertices of the mesh, which are then on the middle surface ω, and $N(A)$ and $N(B)$ the corresponding unit normal vectors. Points A, B and the vector $\gamma \equiv N(A) + N(B)$ define a plane Π which cuts ω along a curve, say AB, that we are aiming

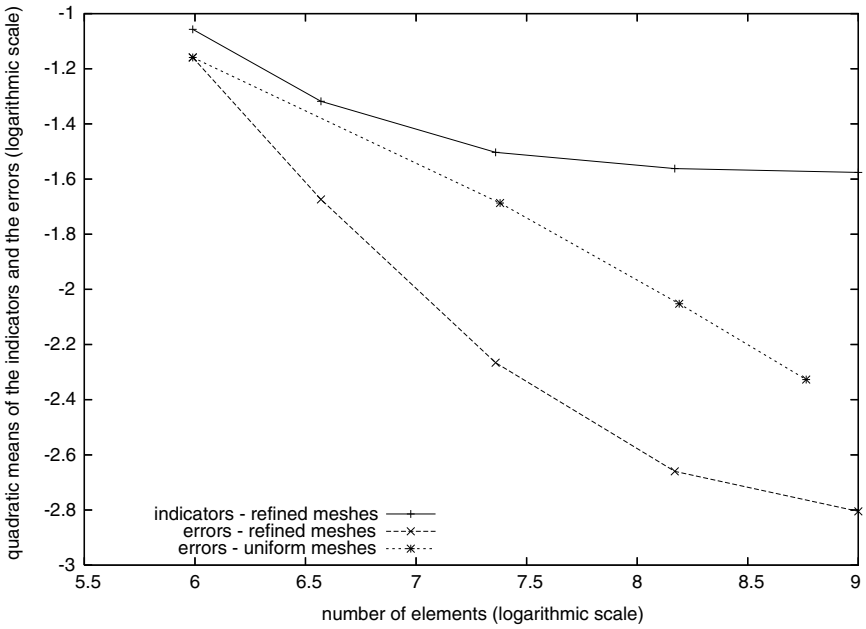

Fig. 10. Cylinder under uniform pressure ($\alpha = 0$) – quadratic means of the error indicators and the "true" errors.

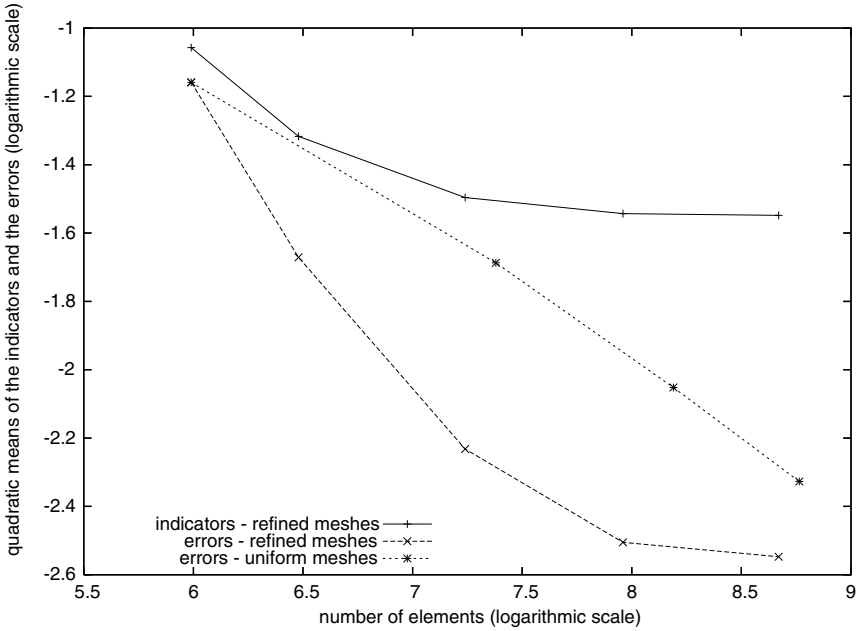

Fig. 11. Cylinder under uniform pressure ($\alpha = 0.25$) – quadratic means of the error indicators and the "true" errors.

at defining an interpolation. First, setting $U = \frac{AB}{\|AB\|}$, a direct orthonormal basis (U, V) of Π is defined. Then, two vectors $T(A)$ and $T(B)$ are introduced, which belong to plane Π, and are, respectively, orthogonal to $N(A)$ and $N(B)$, in such a way that the two vectors T and N define a direct orthonormal basis (see Fig. 5). So, they are tangent to the curve we are trying to construct an interpolation. Now, let k be the euclidian norm of vector AB. We build the third-order polynomial function, say P_3, from $[0, k]$ into $\mathbb{R}$, such that its curve in Π contains A and B, and has $T(A)$ and $T(B)$ as tangent vectors at these points. In other words,

$$P_3(0) = P_3(k) = 0, \quad P_3'(0) = \frac{T_v(A)}{T_u(A)} \equiv \alpha, P_3'(k) = \frac{T_v(B)}{T_u(B)} \equiv \beta,$$

where T_u and T_v stand for the components of vector T in the basis (U, V). Then, it is easy to calculate P_3 as

$$P_3(x) = \alpha x - \frac{2\alpha + \beta}{k} x^2 + \frac{\alpha + \beta}{k^2} x^3.$$

Finally, the new node C is introduced by

$$AC = \frac{k}{2} U + P_3\left(\frac{k}{2}\right) V = \frac{k}{2} U + \frac{k}{8}(\alpha - \beta) V. \tag{11}$$

Remark. In general, the two vertices A and B, and the two normal vectors $N(A)$ and $N(B)$ are not in the same plane. So, in Fig. 5, $\widetilde{N}(A)$ and $\widetilde{N}(B)$ stand for the projection of the exact normal vectors on

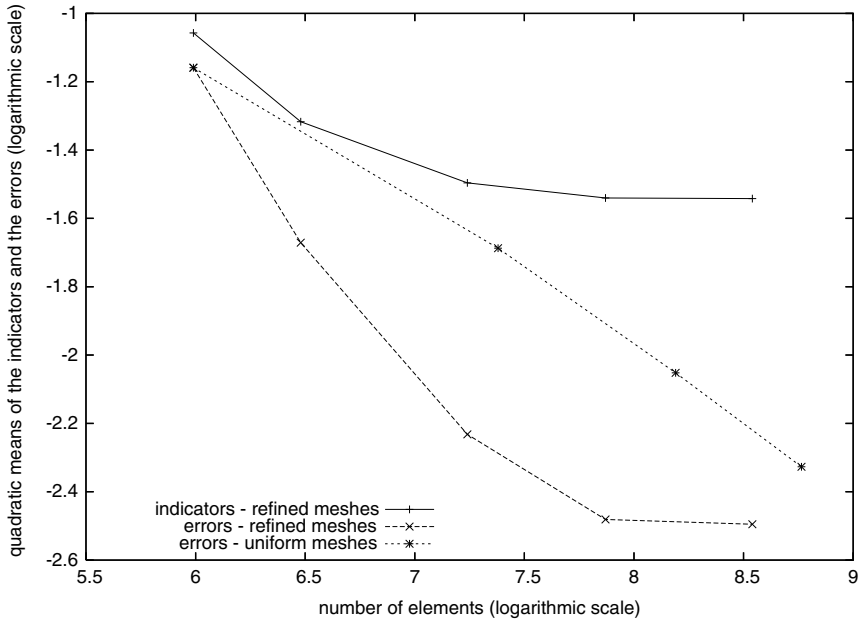

Fig. 12. Cylinder under uniform pressure ($\alpha = 0.5$) – quadratic means of the error indicators and the "true" errors.

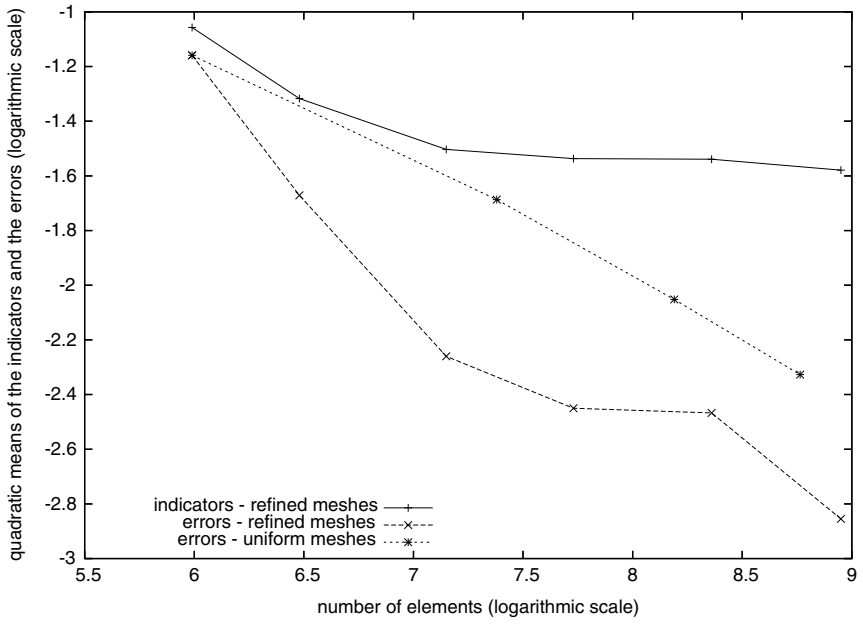

Fig. 13. Cylinder under uniform pressure ($\alpha = 0.75$) – quadratic means of the error indicators and the "true" errors.

the plane Π and are given only for the understanding of the Figure. They are useless for building the function P_3.

Let us now assume that the exact curve $\overset{\frown}{AB}$ can be described by a mapping f, which is assumed to be $\mathscr{C}^4([0,k])$. Then, the previous interpolation procedure is reduced to the well-known Hermite interpolation, for which the error is classical. For all $x \in [0,k]$, there exists $\xi_x \in]0,k[$ such that

$$f(x) - P_3(x) = \frac{x^2(x-k)^2}{24} f^{(4)}(\xi_x).$$

Therefore, if M is a general node of $\overset{\frown}{AB}$ and M_h the node obtained by the above interpolation, the two nodes being of same abscissa in $(A;U,V)$, one has

$$\|MM_h\|_{L^\infty([0,k])} \leqslant \eta_k k^4,$$

where η_k is a constant independent on k but depending on the maximum value of $|f^{(4)}|$ on $[0,k]$ ($f^{(4)}$ is the fourth-order derivative of f). So, when we choose for M the node of abscissa $k/2$, we have $\|MC\| \leqslant \eta_k k^4$. Finally, introducing the mesh parameter h, which is the maximum length of the edges in the mesh, and assuming that the mapping is sufficiently smooth, we can conclude that there exists a strictly positive constant η, independent on h and such that, on the whole mesh

$$\|MC\| \leqslant \eta h^4,$$

where C stands for the added nodes corresponding to the "exact" nodes M.

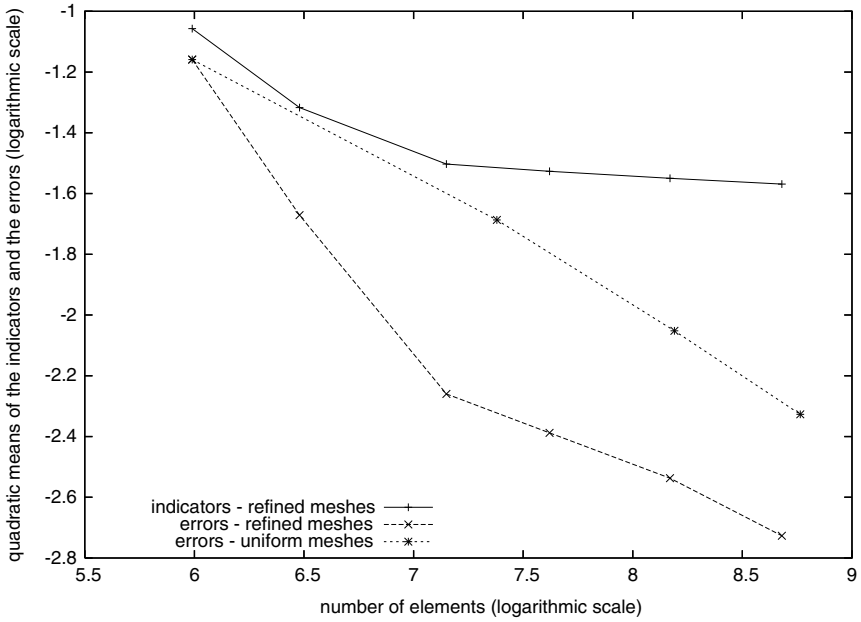

Fig. 14. Cylinder under uniform pressure ($\alpha = 1$) – quadratic means of the error indicators and the "true" errors.

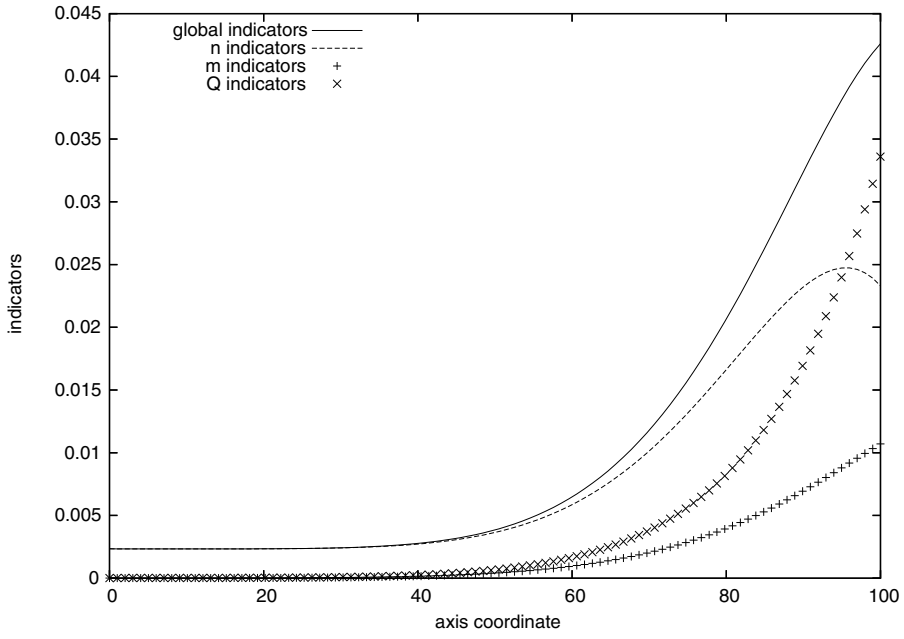

Fig. 15. Cylinder under uniform pressure – first computation – error indicators η, $\eta_n/\sqrt{J_0}$, $\eta_m/\sqrt{J_0}$ and $\eta_q/\sqrt{J_0}$ along the axis direction.

Nevertheless, the geometrical approximation needs also the use of the normal vector. So, a unit normal vector to ω at node C has to be constructed. For this, the classical linear interpolation is used and the vector that has been obtained is normalized:

$$N(C) = \frac{N(A) + N(B)}{\|N(A) + N(B)\|}. \tag{12}$$

In order to obtain an error estimate between $N(C)$ and the exact normal vector $N(M)$ (M is again the node of abscissa $k/2$, previously introduced), let us recall a classical interpolation estimate, applied to our case:

$$\|N - \pi N\|_{L^\infty(\omega)} \leqslant ch^2 \mid N|_{W^{2,\infty}(\omega)}, \tag{13}$$

if π stands for the linear interpolation operator, under classical regularity assumptions on the mesh and if the components of N belongs to $W^{2,\infty}(\omega)$ (see [17]). N represents the unit normal vector. It is homogeneous to the first-order derivatives of the mapping ϕ. Therefore, it is smooth enough because the mapping which defines the surface ω has been assumed to be $\mathscr{C}^3(\hat{\omega})$. Let us also note that the normal vector is defined everywhere on the middle surface ω, because the two tangent vectors have been assumed to be linearly independent at each point of the surface ω. The definition of M ("middle" point of $\widehat{AB}$) leads to

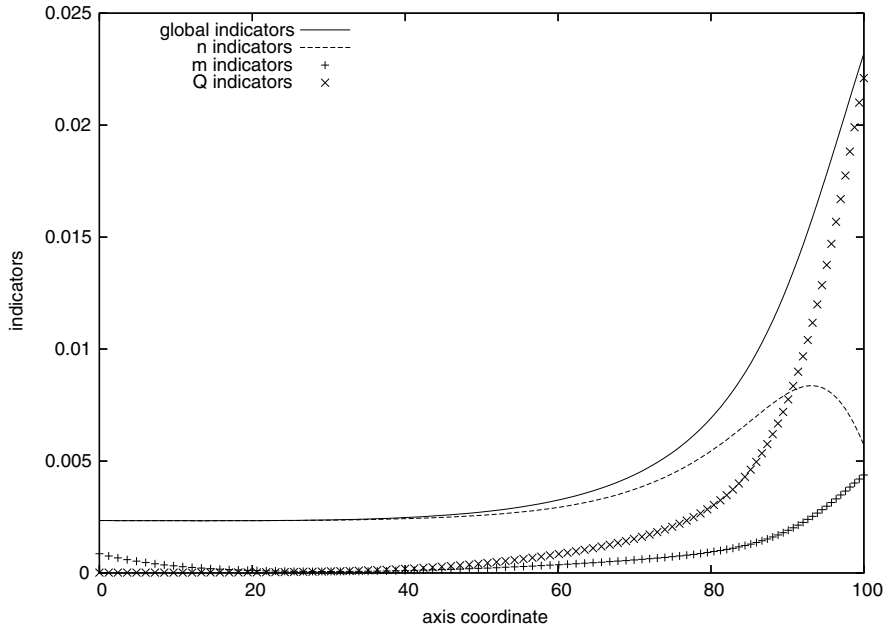

Fig. 16. Cylinder under uniform pressure – first refinement ($\alpha = 0.25$) – error indicators η, $\eta_n/\sqrt{J_0}$, $\eta_m/\sqrt{J_0}$ and $\eta_q/\sqrt{J_0}$ along the axis direction.

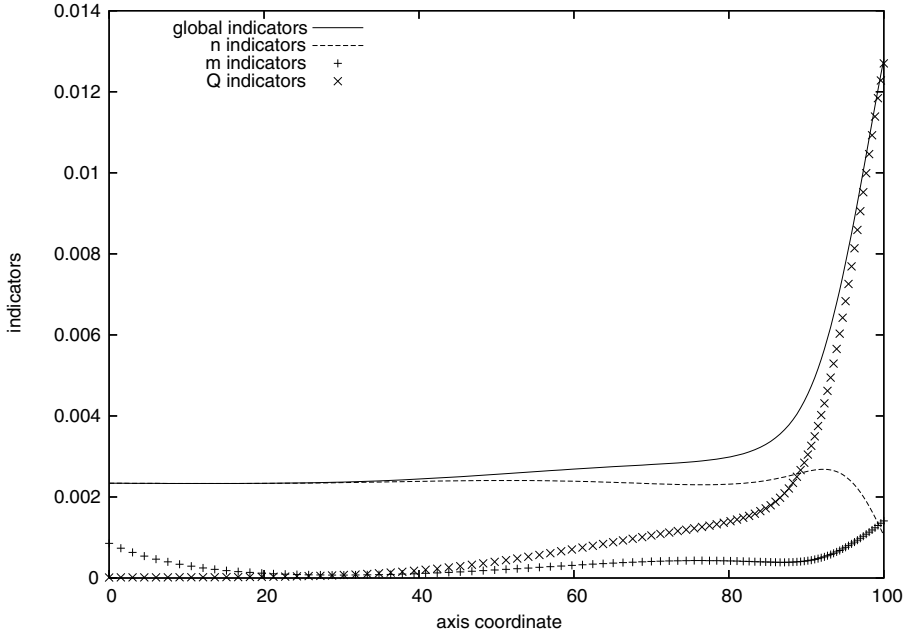

Fig. 17. Cylinder under uniform pressure – second refinement ($\alpha = 0.25$) – error indicators η, $\eta_n/\sqrt{J_0}$, $\eta_m/\sqrt{J_0}$ and $\eta_q/\sqrt{J_0}$ along the axis direction.

$$\pi N(M) = \frac{N(A) + N(B)}{2}.$$

Therefore

$$\begin{aligned}\|\pi N(M)\| &= \|N(M) - N(M) + \pi N(M)\| \\ &\geqslant \|N(M)\| - \|N(M) - \pi N(M)\| \\ &\geqslant \|N(M)\| - \|N - \pi N\|_{L^\infty(\omega)} \\ &\geqslant 1 - ch^2 \mid N|_{W^{2,\infty}(\omega)}\end{aligned}$$

or else

$$1 - \|\pi N(M)\| \leqslant ch^2 \mid N|_{W^{2,\infty}(\omega)}. \tag{14}$$

Moreover, one has

$$\begin{aligned}\|N(M) - N(C)\| &\leqslant \|N(M) - \pi N(M)\| + \|\pi N(M) - N(C)\| \\ &\leqslant \|N - \pi N\|_{L^\infty(\omega)} + \|\pi N(M) - N(C)\|.\end{aligned}$$

Let us remark now that

$$\begin{aligned}\|\pi N(M) - N(C)\| &= \left\| \pi N(M) - \frac{\pi N(M)}{\|\pi N(M)\|} \right\| \\ &= |\ \ \|\pi N(M)\| - 1\ | = 1 - \|\pi N(M)\|,\end{aligned}$$

as

$$\|\pi N(M)\| = \frac{\|N(A) + N(B)\|}{2} \leqslant 1,$$

because the normal vectors are unitary. Finally, using (14), we obtain

$$\|N(M) - N(C)\| \leqslant 2ch^2 \mid N|_{W^{2,\infty}(\omega)}.$$

The previous method was applied on various surfaces, and the numerical results corroborate the above estimates (see [8]).

Remark. Let us observe that this procedure only requires data which are connected to the element edge (coordinates of the two vertices and the two associated normal vectors). It does not depend on the fact that the element is a triangle or a quadrangle. So, it could be applied exactly in the same way for refining meshes made of quadrangles.

5. Mesh refinement criteria

Let us now explain how we choose to refine the mesh. To make it short, the method is based on the smoothing of the elastic energy of the shell. So, a first step is to build new fields of stresses which

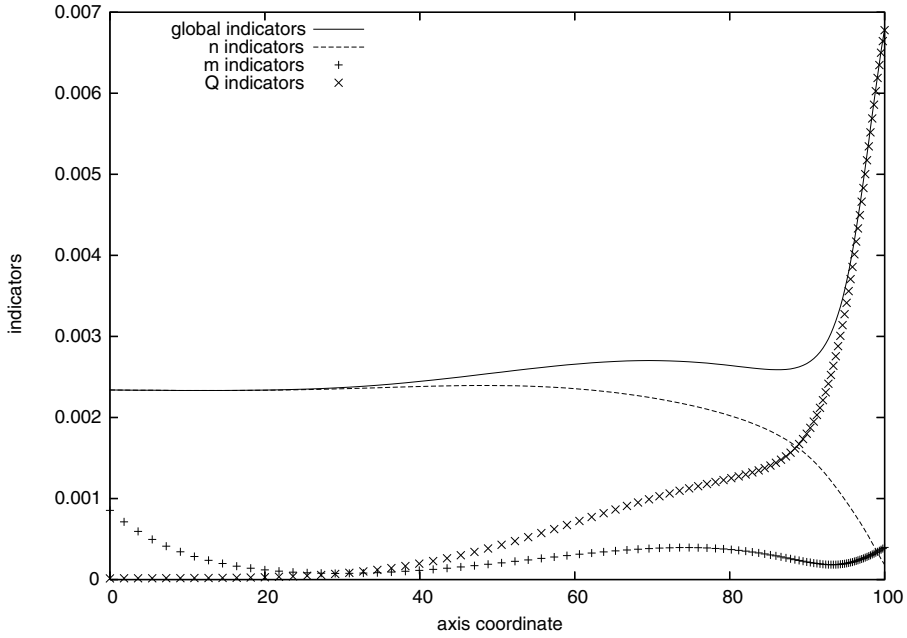

Fig. 18. Cylinder under uniform pressure – third refinement ($\alpha = 0.25$) – error indicators η, $\eta_n/\sqrt{J_0}$, $\eta_m/\sqrt{J_0}$ and $\eta_q/\sqrt{J_0}$ along the axis direction.

length	$L = 6$ m
thickness	$2\varepsilon = 0.03$ m
radius	$R = 3$ m
Young's modulus	$E = 3 \times 10^4$ MPa
Poisson's ratio	$\nu = 0.3$
force	$F = 1$ N

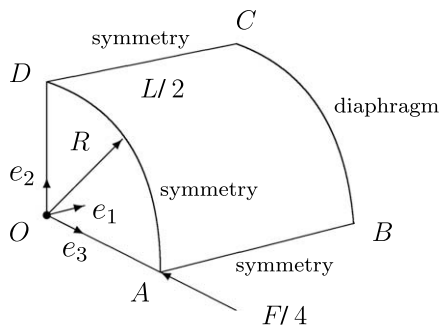

Fig. 19. Settings for the pinched cylinder.

are supposed to give a better approximation of the true ones than the finite element ones. Then, a first part of an error indicator can be obtained thanks to the difference between smoothed and finite element fields. Nevertheless, as shell models are concerned, we have chosen to introduce in our indicator the transverse shear force as a quantity of interest, in a way which is described in the following. On the other hand, though it could certainly be interesting in the framework of shells, in the present paper, we have not introduced an indicator linked with the quality of the geometry approximation, as it is suggested in [7]. Nevertheless, as it will appear further, in most of our test cases, the effect of this approximation has been studied.

5.1. Stress smoothing

First of all, let us notice that the finite element membrane forces tensor n^h and bending moments tensor m^h are constant on each triangle, as first-order polynomial functions are used for the displacements. Moreover, as they are given in a local basis which depends on the element, they have to be expressed in the same global basis (e_1, e_2, e_3) before being smoothed. Then, let us denote by $n^h_{kl}(K)$ and $m^h_{kl}(K)$ the values which are taken on triangle K by any component of n^h and m^h, respectively. Then, at any vertex S of the mesh, we define for any component k and l

$$n^h_{kl}(S) = \frac{\sum_{\mathscr{T}_S} | K | n^h_{kl}(K)}{\sum_{\mathscr{T}_S} | K |}, \quad m^h_{kl}(S) = \frac{\sum_{\mathscr{T}_S} | K | m^h_{kl}(K)}{\sum_{\mathscr{T}_S} | K |}, \tag{15}$$

where $\mathscr{T}_S$ denotes the patch of S, which means the set of elements K which contain the vertex S. Then, the smoothed membrane forces $\tilde{n}^h_K$ and the smoothed bending moments $\tilde{m}^h_K$ are defined as the tensors any component of which is the first-order polynomial functions given on each triangle K by

$$\begin{cases} \tilde{n}^K_{kl} = \sum_{i=1}^{3} n^h_{kl}(S_i)\lambda^K_i, \\ \tilde{m}^K_{kl} = \sum_{i=1}^{3} m^h_{kl}(S_i)\lambda^K_i, \end{cases} \tag{16}$$

where λ^K_i stands for the ith first-order nodal function of K.

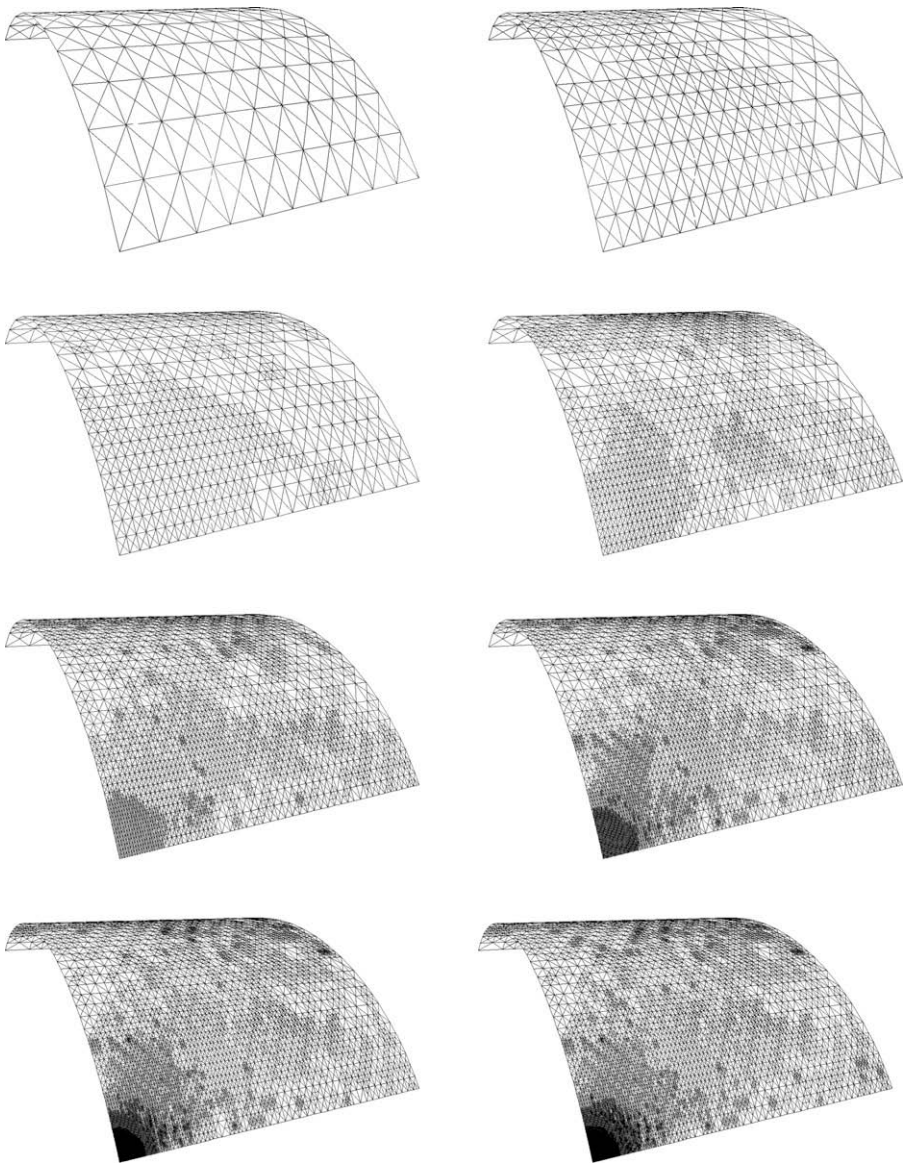

Fig. 20. Successive refinements of the pinched cylinder – $\alpha = 0.25$.

Remark. The values given by (15) are solution of

$$\min_{f\in\mathbb{R}} \int_{\mathscr{T}_S} (f - f_K(X))^2 \, \mathrm{d}X,$$

where $f_K(X)$ is a generic function, which is constant on each element, as in the case of n^h and m^h. Thus, our approach presents several analogies with the one developed by Zhu and Zienkiewicz [9,10]. Let us note yet that we minimize among constants while these authors use first-order degree polynomials.

5.2. Error indication

Let us first recall some basic aspects on the elastic energy J of a general shell model. Let ζ be the linearised strain tensor and σ the stress tensor. The three-dimensional elastic energy reads

$$J = \frac{1}{2}\int_\Omega \sigma : \zeta. \tag{17}$$

Now, the tensors σ and ζ can be splitted into tangential and normal components, such as

$$\zeta = \zeta_t + \zeta_s \otimes N + N \otimes \zeta_s + \zeta_n N \otimes N,$$

and a similar equation for σ. Then, the following decomposition of the elastic energy is derived

$$J = J_t + J_s + J_n \tag{18}$$

with

$$J_t = \frac{1}{2}\int_\Omega \sigma_t : \zeta_t, \quad J_s = \int_\Omega \sigma_s \cdot \zeta_s, \quad J_n = \frac{1}{2}\int_\Omega \sigma_n \zeta_n.$$

The two first quantities are, respectively, the inplane and the transverse shear energies.

In order to recover error indicators homogeneous to an energy, the next step we consider is to express some terms of the decom-

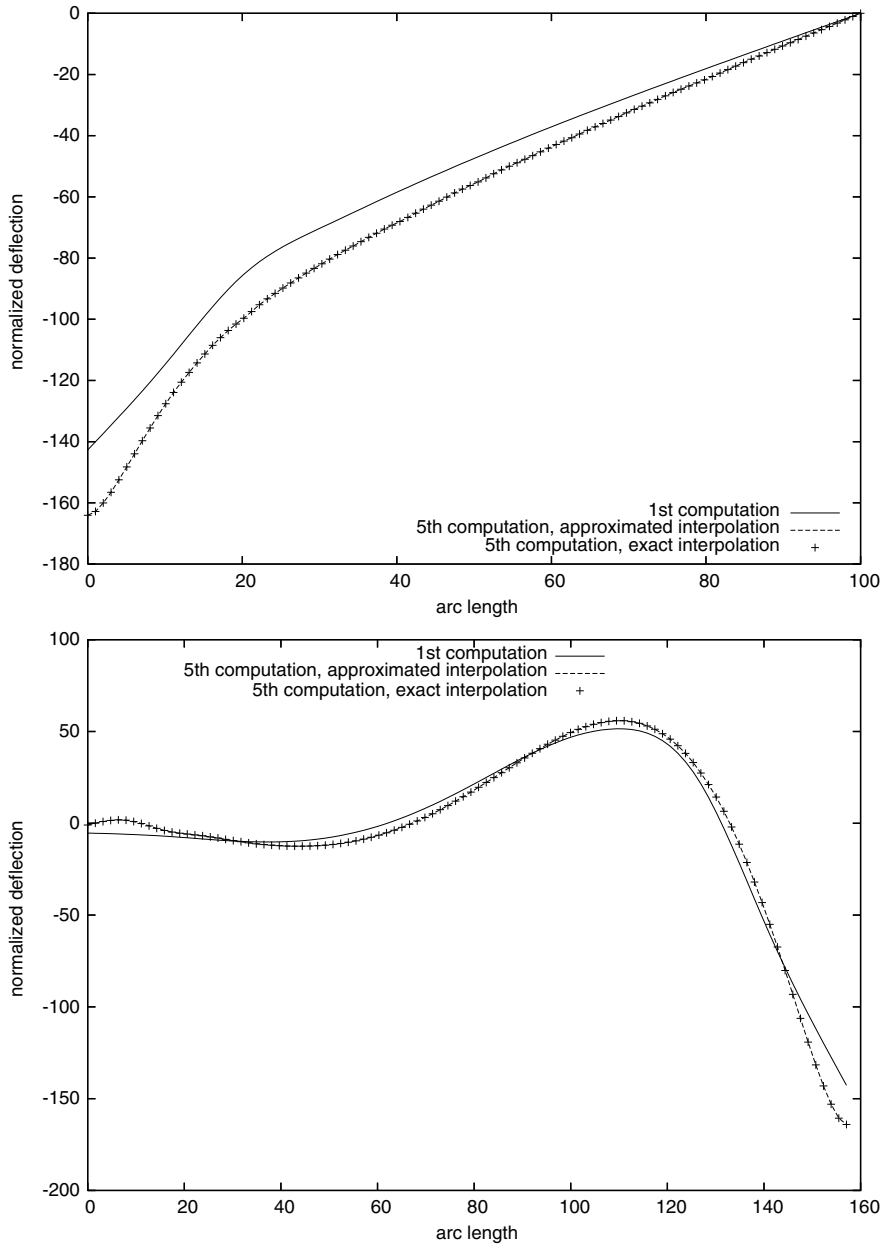

Fig. 21. Pinched cylinder ($\alpha = 0.25$) – normalized deflection along $\widehat{AB}$ (top) and $\widehat{AD}$ (bottom).

position (18) using the forces we are dealing with. Let us first notice that the kinematical hypothesis of the Koiter's shell model leads to

$$\zeta_t = \gamma + x_3\rho, \tag{19}$$

x_3 being the coordinate along the normal direction to the middle surface. Let us recall that γ and ρ are, respectively, the change of metric and the change of curvature tensors previously defined in (4). Then, we get for the inplane strain energy, which is the global elastic energy for our shell,

$$J_t = \frac{1}{2}\int_\omega n : (R^M)^{-1} : n + \frac{\varepsilon^2}{6}\int_\omega m : (R^F)^{-1} : m. \tag{20}$$

Such an expression is appropriate for the smoothing strategy presented in the previous section, and leads naturally to a global error control. But here, we have also chosen to enrich our error indicator with the transverse shear forces. By the way, because of Kirchhoff–Love assumptions, there is no transverse shear energy for the Koiter's or/and Budiansky–Sanders's models. This is due to the fact that the transverse shear strain is zero. Let us observe that Kirchhoff–Love assumptions can be justified thanks to asymptotic methods. It means that the most the shell is thin, the most the transverse shear energy is close to zero. Hence, introducing an energy for the transverse shear in the framework of Kirchhoff–Love's model could appear as not justified in a first time. Nevertheless, first, the "real" thickness of the shells on which engineers work, does not go to zero.

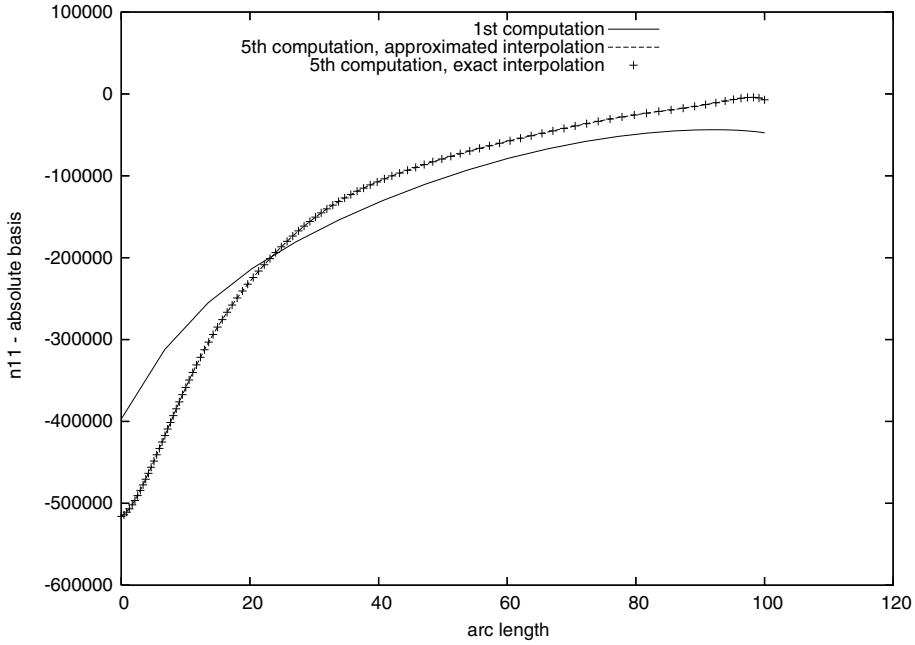

Fig. 22. Pinched cylinder ($\alpha = 0.25$) – n_{11} component in the absolute basis of the resultant stresses along $\widehat{AB}$.

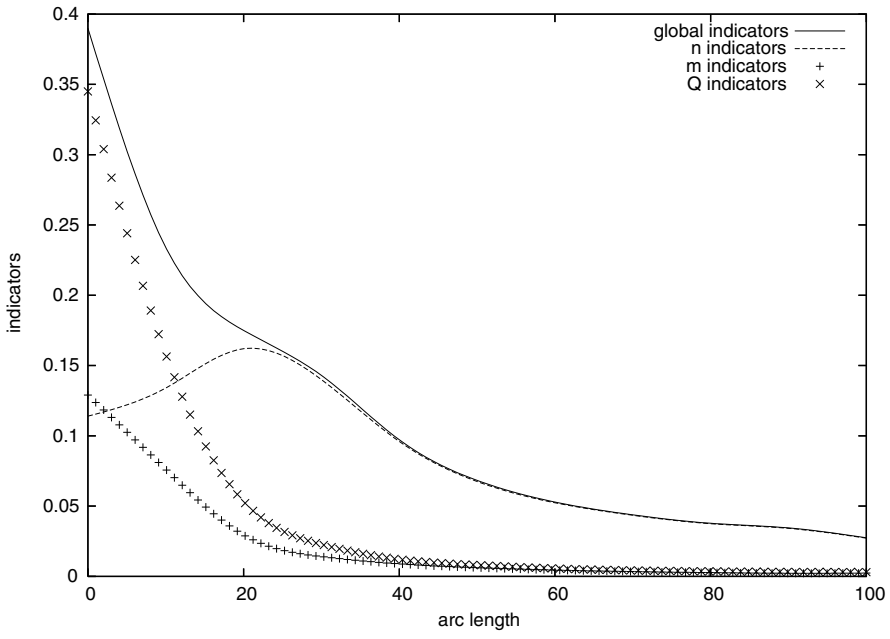

Fig. 23. Pinched cylinder – first computation – error indicators η, $\eta_n/\sqrt{J_0}$, $\eta_m/\sqrt{J_0}$ and $\eta_q/\sqrt{J_0}$ along $\widehat{AB}$.

The thickness can be very small but is not null. And second, in our model, the expression of the Lagrange multiplier can be used to give an indicator on the transverse shear energy. This quantity is of importance when the transverse shear forces take locally big values: it is a way to mean that the shell model becomes questionable and a manner to overcome this, is to refine the mesh locally there. So, from a three-dimensional constitutive law, a resultant transverse energy is defined by

$$I(K) = \frac{1+\nu}{2E\varepsilon}\|\text{grad}\,\varphi + \text{rot}\,\psi\|^2_{L^2(K)} \equiv \frac{1+\nu}{2E\varepsilon}\|q^h\|^2_{L^2(K)}, \tag{21}$$

where φ and ψ are the two potential functions used in the definition of the transverse shear forces (see (7)).

The previous considerations lead us to define error indicators for each type of forces by

$$\begin{cases} \eta_n(K) = \sqrt{\frac{1-\nu^2}{2E\varepsilon}}\|\tilde{n}^h - n^h\|_{L^2(K)}, \\ \eta_m(K) = \sqrt{\frac{\varepsilon(1-\nu^2)}{6E}}\|\tilde{m}^h - m^h\|_{L^2(K)}, \\ \eta_q(K) = \sqrt{I(K)}. \end{cases} \tag{22}$$

In order to define a relative error indicator, the following quantity is introduced

$$J_0 = \sum_{K\in\mathcal{T}_0}\left\{\frac{1-\nu^2}{2E\varepsilon}\|\tilde{n}^h\|^2_{L^2(K)} + \frac{\varepsilon(1-\nu^2)}{6E}\|\tilde{m}^h\|^2_{L^2(K)} + \frac{1+\nu}{2E\varepsilon}\|q^h\|^2_{L^2(K)}\right\},$$

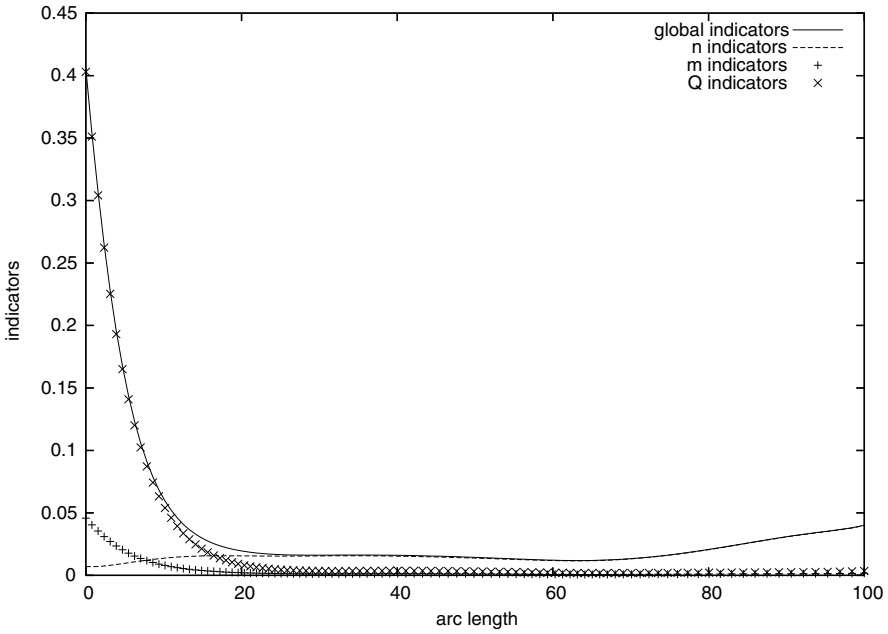

Fig. 24. Pinched cylinder – second refinement ($\alpha = 0.25$) – error indicators η, $\eta_n/\sqrt{J_0}$, $\eta_m/\sqrt{J_0}$ and $\eta_q/\sqrt{J_0}$ along $\widehat{AB}$.

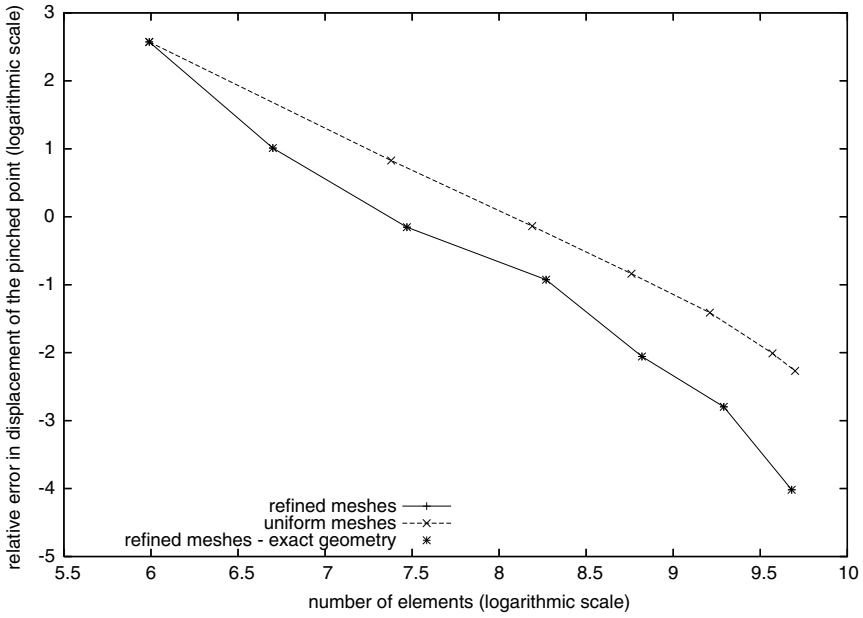

Fig. 25. Pinched cylinder ($\alpha = 0.25$) – relative error (%) of the displacement of the pinched point, in logarithmic scale (reference value: −164.24) – refined and uniform meshes with exact geometry.

where $\mathscr{T}_0$ is the mesh used for the initial computation. The local error indicator then reads

$$\eta(K) = \sqrt{\frac{\eta_n^2(K) + \eta_m^2(K) + \eta_q^2(K)}{J_0}}. \tag{23}$$

Finally, the refinement of a triangle K is effective when one has, for a given positive or null α,

$$\eta(K) > \eta_{\text{mean}} + \alpha s, \tag{24}$$

where η_{mean} and s stand, respectively, for the arithmetic mean and standard deviation of error indicators. In general, the larger is α, the more concentrated will be mesh refinement. In fact, the values of this parameter influence the decrease of the global estimation during the refinement process, as shown later.

6. Numerical experiments

Some numerical results testing the approach previously described, are presented now. Among them are classical shell problems, for which reference solutions are described in the literature (see e.g., [22]). They allow us to check the computation accuracy when the number of elements increases while refining the mesh. In particular, the following points, which we found interesting in our approach, will be examined.

- *What is the effect of the geometry approximation on the computation accuracy after a few refinement iterations?*
  Thus, when it is possible, it will be worthwhile to consider the case of the exact interpolation in order to compare the results with the approximated interpolation ones.
- *Are the error indicators of the different stresses such that each of them can play a role in the refinement process?*
  If it is, it will justify the weights chosen in (22).
- *Is the error indicators behaviour close to the one of the "true" errors?*
  This can be investigated when an analytical solution of the problem is available, as in the first case considered underneath. It should be noticed that the effectivity index is classically used to answer to this question (see e.g., [23]). Let us remember that the main goal of the indicator suggested here is to detect where to refine in order to obtain a good accuracy for the transverse shear forces. It is not designed to be close to the "true" error.

length	$L = 12$ m
thickness	$2\varepsilon = 0.32$ m
width	$b = 1.1$ m
Young's modulus	$E = 29$ MPa
Poisson's ratio	$\nu = 0.22$
force	$F = 1$ N

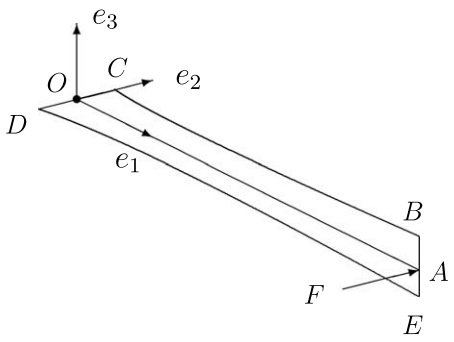

Fig. 26. Settings for the twisted ribbon.

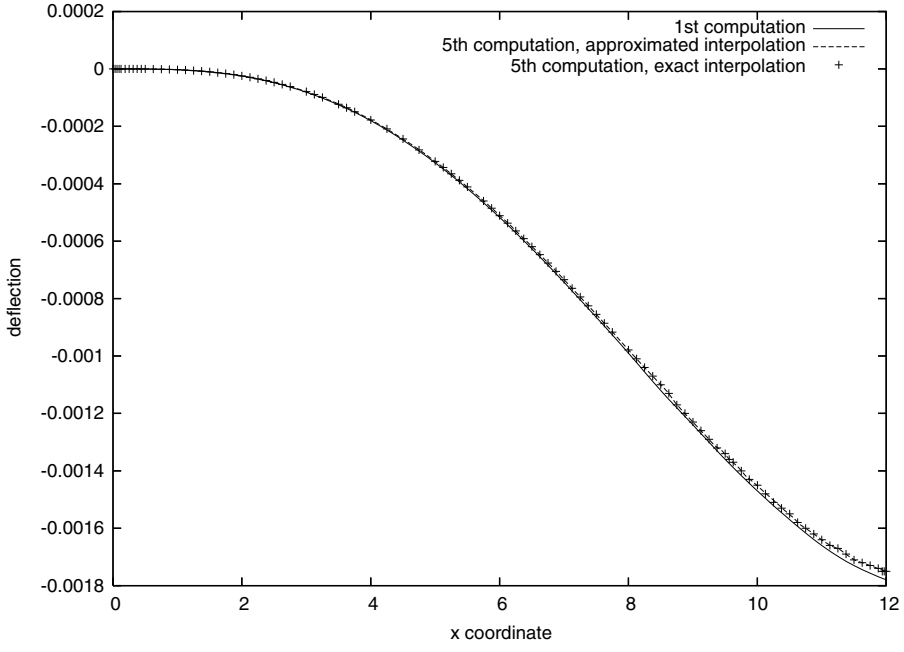

Fig. 27. Twisted ribbon ($\alpha = 0.5$) – deflection along $\widehat{DE}$.

6.1. Cylinder under uniform pressure

Let us begin with the case of a cylindrical shell, which is clamped on one side, the opposite one being free. It is submitted to an internal uniform pressure load P. Thus, the shell and the load are both axisymmetric. So, the solution depends only on the abscissa along the shell axis, say ξ^2, in the case of the mapping

$$\phi(\xi^1, \xi^2) = \begin{pmatrix} \xi^2 \\ R\cos\xi^1 \\ R\sin\xi^1 \end{pmatrix}, \tag{25}$$

where R is the radius of the cylinder. The main interest of this example is that the exact solution of the Koiter's model can be easily obtained (see [24]).

In the local basis given by (25), the membrane forces tensor n is such that

$$n_1^1 = \frac{2E\varepsilon}{R} u_3,$$

its other components being zero, and the bending moments are

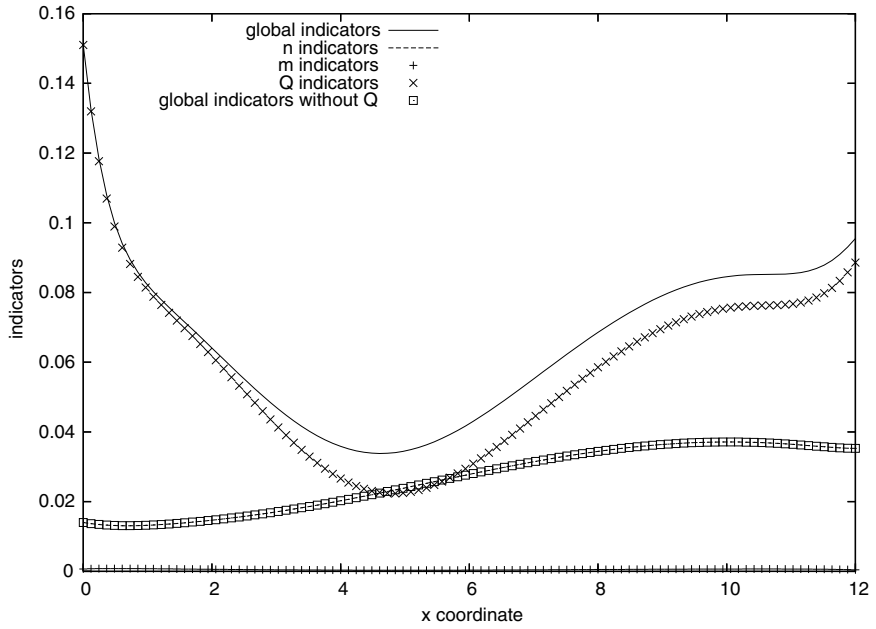

Fig. 28. Twisted ribbon – first computation. Error indicators $\eta, \eta_n/\sqrt{J_0}, \eta_m/\sqrt{J_0}$ and $\eta_q/\sqrt{J_0}$ along $\widehat{DE}$. The local indicators computed without the contribution of $\eta_q/\sqrt{J_0}$ are also presented.

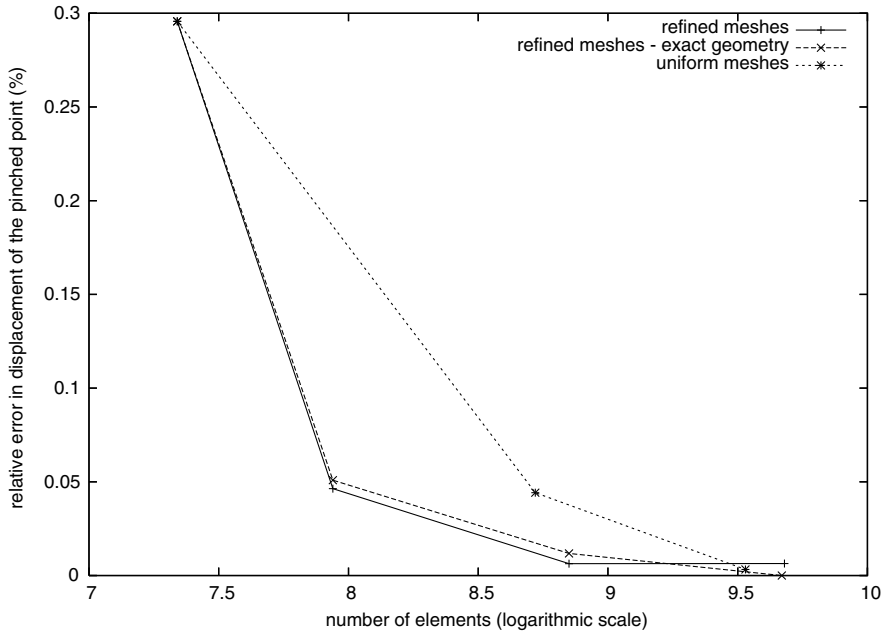

Fig. 29. Twisted ribbon ($\alpha = 0.5$) – relative error (%) of the displacement of the pinched point (reference value: 1.7493×10^{-3}) – refined and uniform meshes with exact geometry.

geometrical parameters	$b = 0.5$ m
	$c = 0.1$ m
thickness	$2\varepsilon = 0.008$ m
Young's modulus	$E = 2794.895$ MPa
Poisson's ratio	$\nu = 0.4$
pressure	$P = 980.665$ Pa

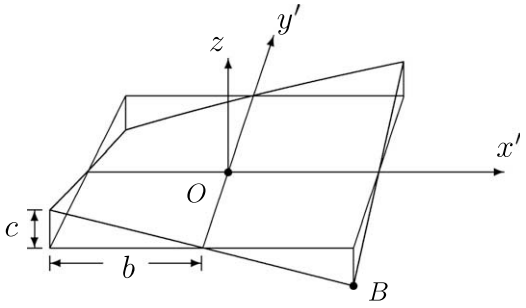

Fig. 30. Settings for the hyperbolic paraboloid.

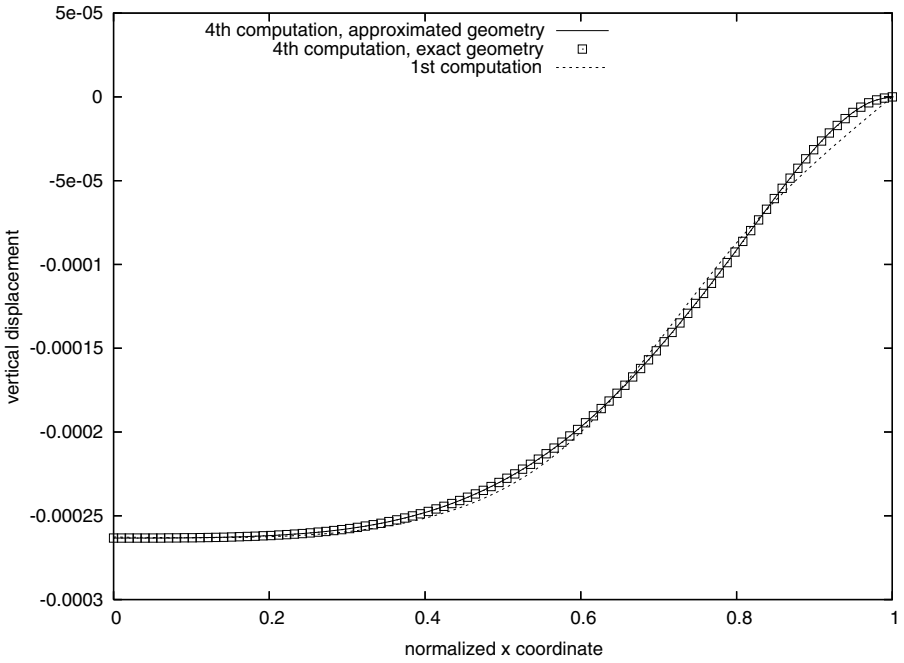

Fig. 31. Hyperbolic paraboloid – vertical displacement of $\widehat{OB}$.

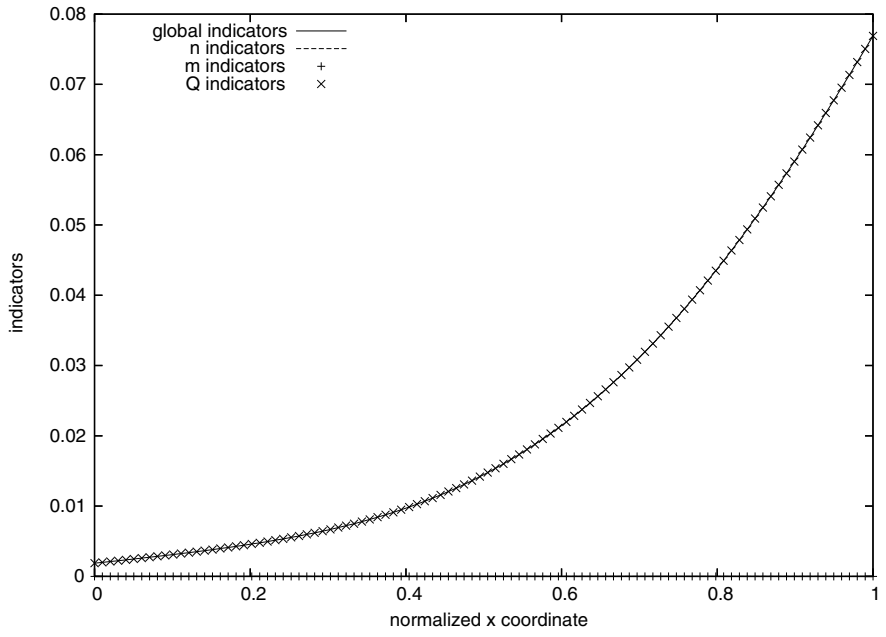

Fig. 32. Hyperbolic paraboloid – first computation – error indicators η, $\eta_n/\sqrt{J_0}$, $\eta_m/\sqrt{J_0}$ and $\eta_q/\sqrt{J_0}$ along $\widehat{OB}$.

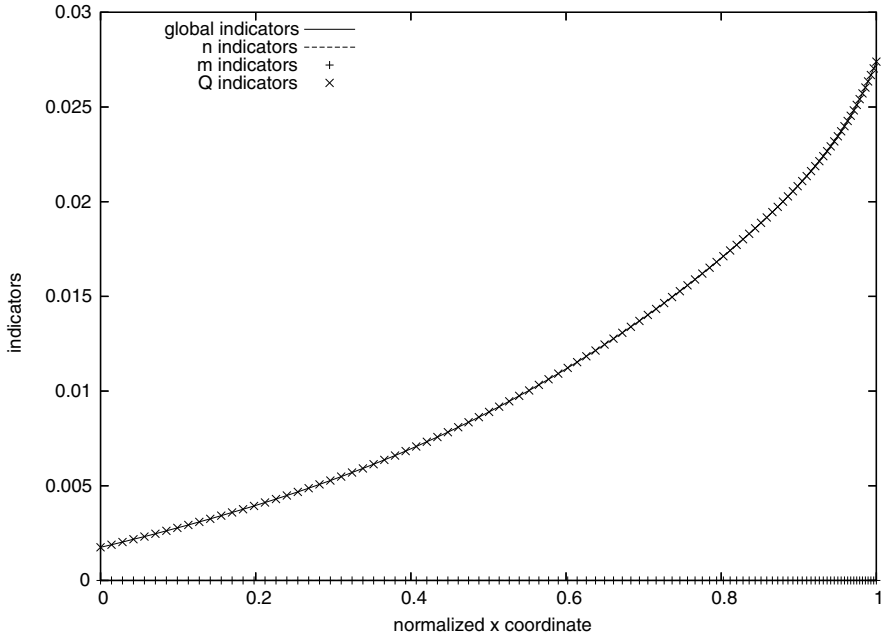

Fig. 33. Hyperbolic paraboloid – second refinement ($\alpha = 0$) – error indicators η, $\eta_n/\sqrt{J_0}, \eta_m/\sqrt{J_0}$ and $\eta_q/\sqrt{J_0}$ along $\widehat{OB}$.

Table 2
Settings for the tank under uniform pressure – geometrical aspects

Length of the cylinder	Thickness	Radius of the cylinder and hemispheres
$L = 25.132$ m	$2\varepsilon = 0.02$ m	$R = 10$ m

Table 3
Settings for the tank under uniform pressure – mechanical aspects

Young's modulus	Poisson's ratio	Internal pressure
$E = 68.25 \times 10^6$ Pa	$\nu = 0.3$	$P = 3 \times 10^3$ Pa

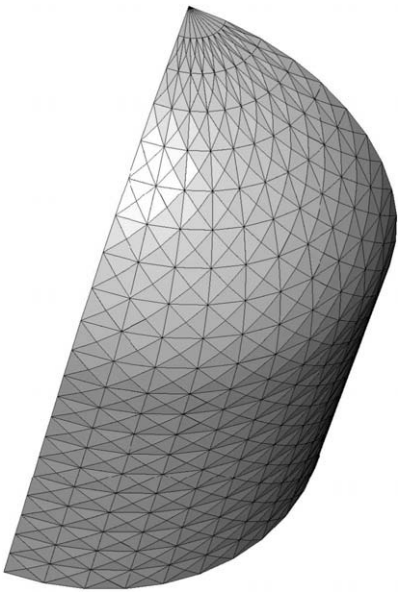

Fig. 34. Tank under uniform internal pressure – one eighth of the structure.

$$\begin{cases} m_1^1 = -\frac{2E\varepsilon}{1-\nu^2}\left(\frac{1}{R^2}u_3 + \nu u_{3,22}\right), \\ m_2^2 = -\frac{2E\varepsilon}{1-\nu^2}\left(\frac{\nu}{R^2}u_3 + u_{3,22}\right), \end{cases}$$

while $m_1^2 = m_2^1 = 0$. Then the transverse shear forces read

$$q^1 = 0, q^2 = m_{,2}^{22}.$$

Finally, the knowledge of the deflection u_3 allows us to compute all these forces. This can be done by solving the following differential equation:

$$\begin{cases} \frac{2E\varepsilon^3}{3(1-\nu^2)}\left\{u_{3,2222} + \frac{2\nu}{R^2}u_{3,22} + \left(\frac{1}{R^2} + \frac{3(1-\nu^2)}{\varepsilon^2}\right)\frac{u^3}{R^2}\right\} = P, \\ u_3(L) = 0, \quad u_{3,2}(L) = 0, \quad m_2^2(0) = 0, \quad m_{2,2}^2(0) = 0, \end{cases} \tag{26}$$

where L is the cylinder length. The settings for the computation are given in Table 1.

One observes in Figs. 6–9 the very good accuracy of the numerical solution versus the analytical one, after four refinements, even for the bending moments and the transverse shear forces, especially near the clamped edge.

Finally, an approximated "true" error for this test-problem can be derived. To achieve this, the difference between the analytical values of the forces at the vertices of the mesh and the finite element forces is evaluated in a similar way than in (21) and (22). More precisely, we set for each triangle K:

$$\begin{cases} \widetilde{n}_K^a = \sum_{i=1}^{3} n_{S_i}^a \lambda_i^K, \\ \widetilde{m}_K^a = \sum_{i=1}^{3} m_{S_i}^a \lambda_i^K, \\ \widetilde{q}_K^a = \sum_{i=1}^{3} q_{S_i}^a \lambda_i^K, \end{cases} \tag{27}$$

where $n_{S_i}^a, m_{S_i}^a$ and $q_{S_i}^a$ are, respectively, the analytical exact membrane forces, bending moments and shear forces computed at node S_i, while λ_i^K is, as in (16), the ith first-order nodal function of K. Then, the approximated "true" error is defined as

$$e(K) = \sqrt{\frac{e_n^2(K) + e_m^2(K) + e_q^2(K)}{J_0^a}}, \tag{28}$$

where

$$\begin{cases} e_n(K) = \sqrt{\frac{1-\nu^2}{2E\varepsilon}} \|\widetilde{n}^a - n^h\|_{L^2(K)}, \\ e_m(K) = \sqrt{\frac{\varepsilon(1-\nu^2)}{6E}} \|\widetilde{m}^a - m^h\|_{L^2(K)}, \\ e_q(K) = \sqrt{\frac{1+\nu}{2E\varepsilon}} \|\widetilde{q}^a - q^h\|_{L^2(K)}, \end{cases} \tag{29}$$

and

$$J_0^a = \sum_{K \in \mathscr{T}_0} \left\{ \frac{1-\nu^2}{2E\varepsilon} \|\widetilde{n}^a\|^2_{L^2(K)} + \frac{\varepsilon(1-\nu^2)}{6E} \|\widetilde{m}^a\|^2_{L^2(K)} + \frac{1+\nu}{2E\varepsilon} \|\widetilde{q}^a\|^2_{L^2(K)} \right\}.$$

Fig. 11 allows one to compare the error indicators with the estimated "true" errors, as the mesh is refined. The decrease rate of the quadratic mean values of the errors is more important than the one of the indicators. This behaviour is due to the fact that the transverse shear forces are compared to zero in our indicator. However, they are locally very large near the clamped edge (see Fig. 9). Then, the mixed model introduced in Section 3 combined with our mesh refinement criteria allows one to refine the mesh where the transverse shear forces are important and to obtain a good accuracy on them. Moreover, Fig. 11 illustrates also the efficiency of the mesh refinement compared to a uniform mesh refinement.

The comparison of Figs. 10 to 14 shows how the selectivity parameter α introduced in (24) influences the decrease rate of the error indicators and the "true" errors. For large values of α, the decrease rate can be irregular.

Finally, one can describe more precisely the effects of each part of the error indicator. Thus, $\eta_n/\sqrt{J_0}, \eta_m/\sqrt{J_0}, \eta_q/\sqrt{J_0}$ and the local indicator η along the axis direction, for the initial computation and after 1, 2 and 3 refinement iterations, are shown in Figs. 15–18. In all the cases, most of the error concentrates near the clamped edge. Nevertheless, the effect of each indicator does not follow the same way. The membrane forces indicator rapidly decreases near the clamped edge and remains dominant far from it. Near the clamped edge, the transverse shear forces indicator becomes more and more important, relatively to the two other ones, and finally selects the refinement area. The effect of the bending moment indicator is rather weak. It also decreases rapidly near the clamped edge and increases near the free edge. The reason is that, when the Koiter's shell model is used, a local deformation of the shell occurs near the free edge, due to bending moments. Let us finally observe that the global error does not change far from the clamped edge, because the mesh refinement concentrates near this edge. Dropping the transverse shear forces indicator away from the local indicator would completely change the refinement strategy as the global error would concentrate far from the clamped edge.

6.2. Pinched cylinder

Here, a cylindrical shell is simply supported at its extremities by two diaphragms and loaded by two opposite pointwise forces F and $-F$ in the middle. Because of the problem symmetry, only one eighth of the cylinder is generally considered where the force $F/4$ is applied (see Fig. 19).

An analytical solution, which is used as a reference one for this problem, is obtained using a double Fourier series and the relations due to Flügge (see [25]). But it does not correspond exactly to the Koiter's model, for which the change of curvature tensor is slightly different. So, this so-called reference value for the normalized deflection at the pinched point is $\frac{2E\varepsilon u_3}{\|F\|} = -164.24$. When starting from a uniform mesh of 400 elements, we get -164.21 at the 7th computation (see Fig. 20). Let us note that this value does not vary significantly when using finer meshes. Therefore, it can be said that convergence has been obtained for our model.

In a similar way, concerning the stresses, a reference normalized value of the component n_{11} of the membrane force in the absolute basis at the pinched point is $\frac{Rn_{11}}{\|F\|} = -15.72$, while we get -17.3.

The approximated interpolation of vertices and normal vectors, described in Section 4.3, generates a neglectible error for the

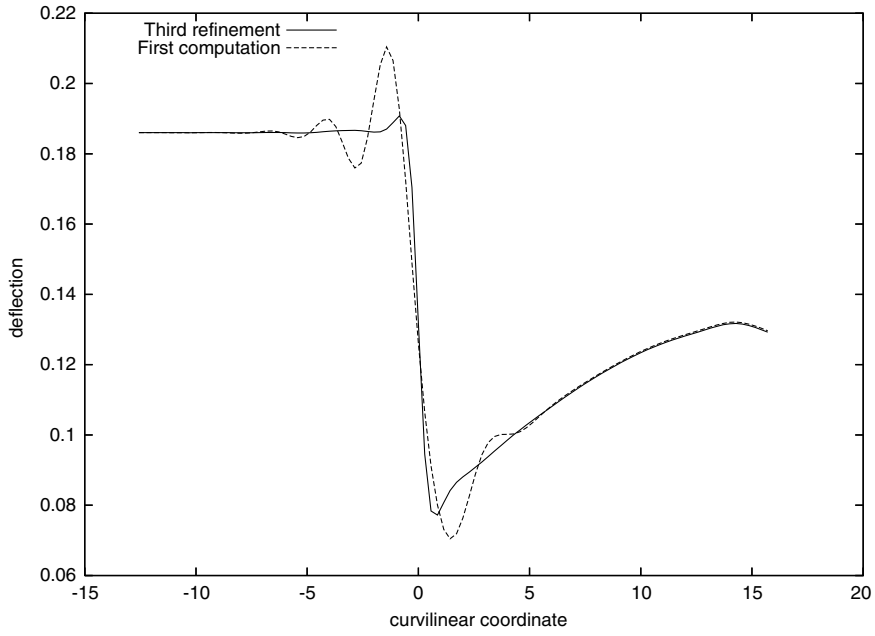

Fig. 35. Tank under uniform internal pressure – normal displacement along the axis direction of the computational domain. The coordinates of the junction and the hemisphere top are 0.0 and 15.8, respectively.

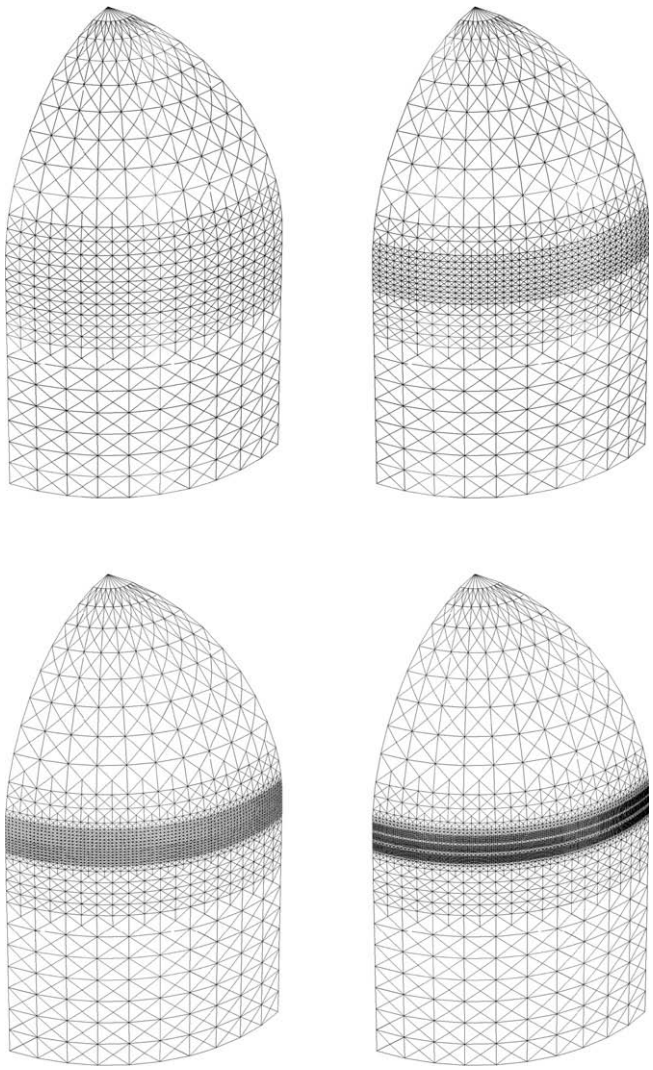

Fig. 36. Tank under uniform internal pressure ($\alpha = 0$) – successive refinements.

deflection, as shown in Fig. 21. It is worth to note that the conclusion is the same for the stresses (see Fig. 22).

Finally, the error indicators $\eta_n/\sqrt{J_0}$, $\eta_m/\sqrt{J_0}, \eta_q/\sqrt{J_0}$ along $\overset{\frown}{AB}$ and the local indicator η are shown in Fig. 23. It can be observed that the membrane forces indicator is dominant away from the pinched point, while near this point the bending moment and the transverse shear forces indicators grow and finally contribute to select the refinement area. The same features remain valid after more refinement iterations (see Fig. 24). For these computations, our goal is reached because η_n, η_m and η_q are weighted in such a manner that none of them masks systematically the others during the refinement process. A last point that should be noticed is the efficiency of the mesh refinement versus a uniform mesh refinement, as shown in Fig. 25.

6.3. Pinched twisted ribbon

Let us now consider another instructive classical example: the twisted cantilevered ribbon (see Fig. 26). One extremity is clamped and the opposite one is submitted to a concentrated unit shear load in the thickness direction.

The computed displacement for the pinched point A in the basis (e_1, e_2, e_3) is $(0., 0.00175, -0.00171)$ at the 5th computation as the reference solution given by [22] is $(0., 0.00175, -0.00179)$, this solution being derived from the beam theory.

The error indicators $\eta, \eta_n/\sqrt{J_0}, \eta_m/\sqrt{J_0}$ and $\eta_q/\sqrt{J_0}$ along $\overset{\frown}{DE}$ are shown in Fig. 28. Let us remark that the transverse shear and the membrane forces indicators lead to the same order of magnitude. Although the bending moment drops back in this case, the weights of (22) are satisfying.

Finally, Fig. 27 shows the good accuracy along $\overset{\frown}{DE}$ of the approximated interpolation method proposed in [8], while Fig. 29 reveals, at the pinched point, the approximated interpolation gives slightly less accurate results than the exact one. To overcome this problem, it could be advantageous to incorporate some shell geometrical informations to the error indicator (see [7] for an example of such an approach).

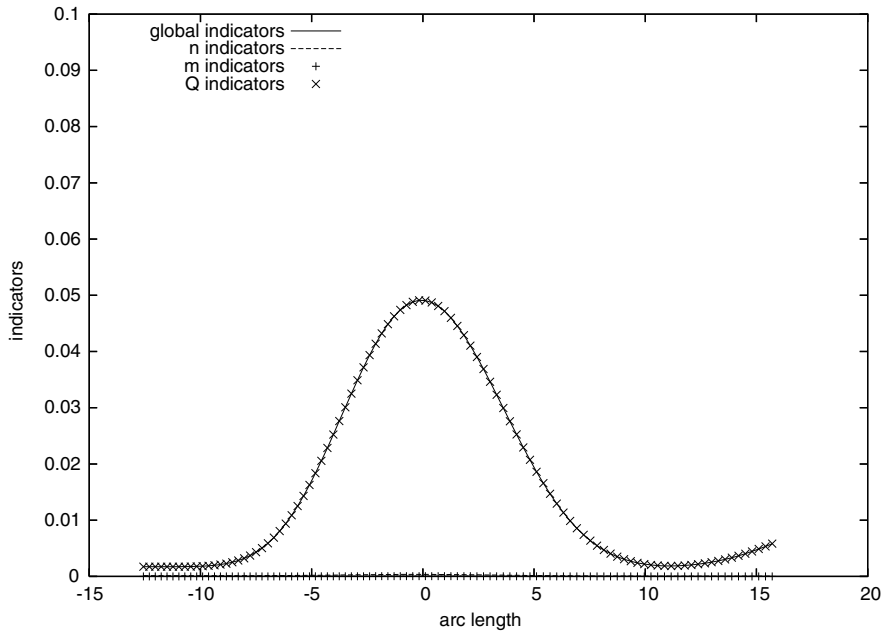

Fig. 37. Tank under uniform internal pressure – first computation. Error indicators $\eta, \eta_n/\sqrt{J_0}, \eta_m/\sqrt{J_0}$ and $\eta_q/\sqrt{J_0}$ along the axis direction of the computational domain.

6.4. Clamped hyperbolic paraboloid

The middle surface is given by the mapping

$$\phi(\xi^1,\xi^2)=\begin{pmatrix}\xi^1-b\\ \xi^2-b\\ \frac{c}{2b^2}((\xi^2)^2-(\xi^1)^2)\end{pmatrix}, \tag{30}$$

where b and c are two positive numbers and $\hat{\omega}=]0,2b[\times]0,2b[$ (see Fig. 30, where the frame $Ox'y'$ is obtained from Oxy by the rotation of $\pi/4$ radians in this plane). The geometrical and mechanical settings are those of the case described in e.g., [26].

First, let us notice that the displacement of the center point O is close to the reference solution given in [26]. For the clamped parabolic hyperboloid, the refinement concentrates near the boundaries. The clamped boundary condition, which creates a horizontal tangency along the edge, appears clearly on the deformed configuration after few refinements, as shown in Fig. 31. Again, exact and approximated interpolations give very close results.

Figs. 32 and 33 show that the refinement process is strongly dependant on the transverse shear forces indicator η_q for the clamped hyperbolic paraboloid. This underlines again the importance of η_q in the expression (23) of the error indicator.

6.5. A case of junction of shells: tank under uniform pressure

As a more complex structure than the previous ones, a shell which contains junctions between a cylinder and two hemispheres is now considered. The mechanical load is an internal uniform pressure. The data are given in Tables 2 and 3. Due to the problem symmetry, only one eighth of the structure is considered (see Fig. 34).

An analytical solution is available in [24] for the tank under uniform pressure. However, the hemispheres are considered as two membranes and the shell model of the cylinder is Novozhilov's one, which is different from Koiter's model, even if it belongs to the same family of Kirchhoff–Love's models. Consequently, this analytical solution is too different from ours to take the role of the reference solution. However, let us mention that on the spherical side of the structure, the "analytical" normal displacement near the junction is $u_3=\frac{(1-\nu)pR^2}{4eE}=0.07692$, as we get $u_3=0.08783$ (see Fig. 35), whereas on the cylindrical side of the structure, the "analytical solution" gives $u_3=0.18853$ while we get $u_3=0.19092$. Thus, the analytical results indicate that the deflection variation has to be located at the junction. This can be observed in Fig. 35. Furthermore, Fig. 36 shows, as expected, the location of the refinement in the vicinity of the junction. Correspondingly, the error indicators concentrate on the junction during the refinement process (see Fig. 37, the results remain the same after several iterations). Finally, the good results of the approximated interpolation and the interest of a refinement strategy versus a uniform mesh refinement are illustrated in Fig. 38.

6.6. A case of cracked shell

The last test-problem considered in this paper is a cracked cylindrical shell. One quarter of a cylinder is clamped on all its boundary and submitted to a uniform pressure. The settings are those of Table 1. Let us note that the crack was chosen so that its

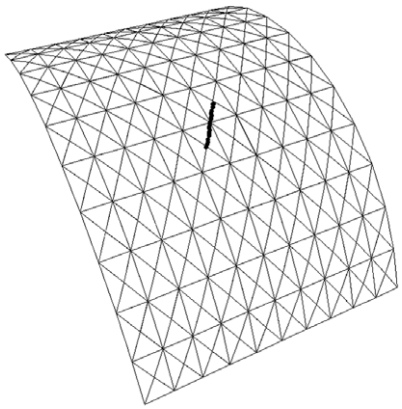

Fig. 39. Cracked cylindrical shell – location of the crack on the initial mesh.

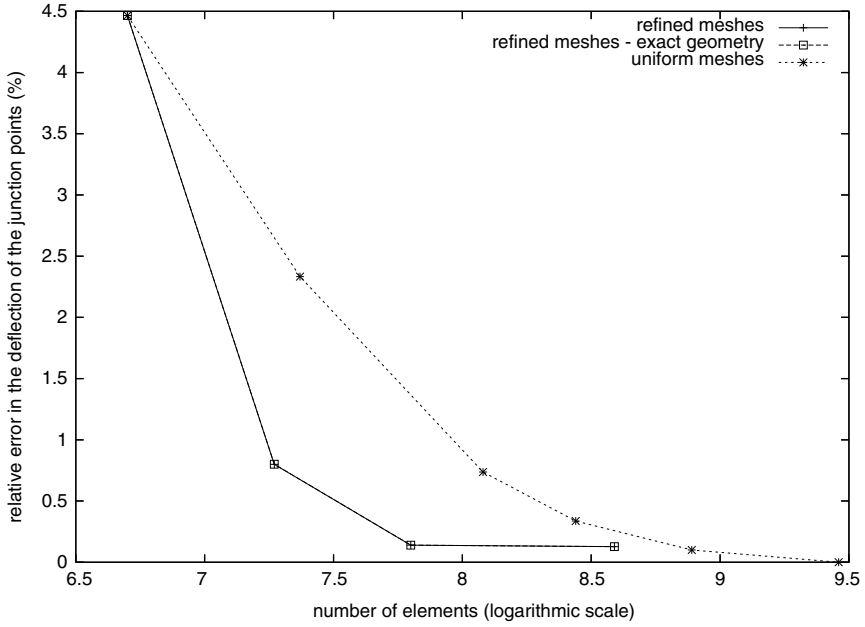

Fig. 38. Tank under uniform internal pressure ($\alpha=0$) – relative error (%) of the deflection of the junction points (reference value: 0.1319 m) – refined and uniform meshes with exact geometry.

direction is not along the principal directions of curvature of the middle surface (see Fig. 39).

It can be observed in Fig. 40 that the refinement propagates partially in an orthogonal direction of the crack.

All error indicators decrease near the crack tip during the refinement process (see Fig. 41). The structure carries the load dominantly by membrane action. Thus, the membrane forces indicator is highly dominant. In the studied case, the opening mode is Mode I, for which the stresses are the most important in a direction which is perpendicular to the crack: it explains the refinement propagation. Finally, it can be observed that, as expected, the stresses increase near the crack tip, which is in fact theoretically singular (see Fig. 42). Here the stresses are evaluated in L^2 norm on the patch of the crack tip.

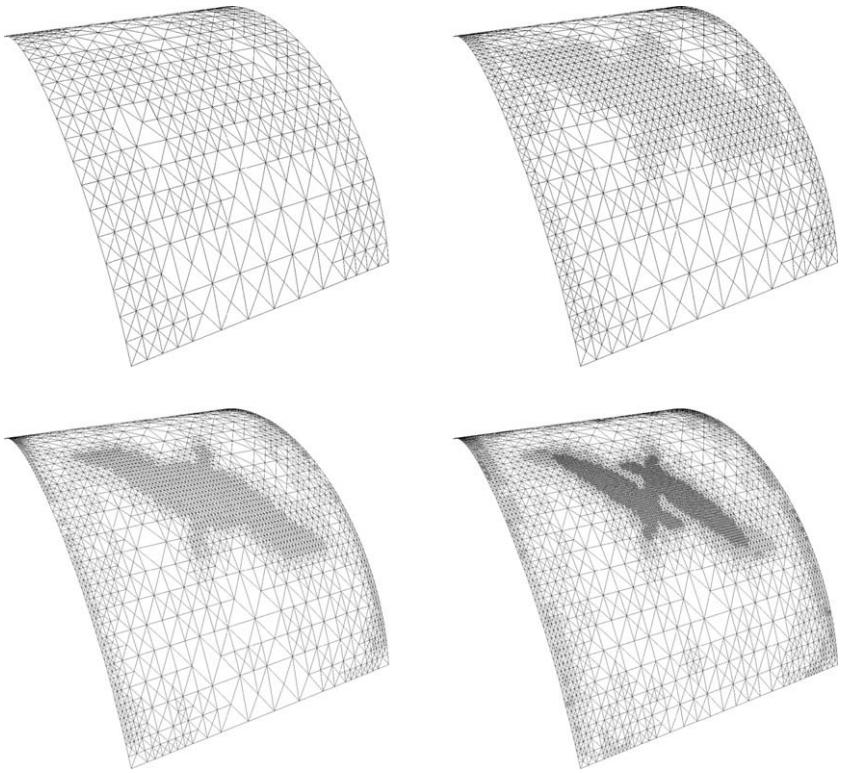

Fig. 40. Cracked cylindrical shell ($\alpha = 0$) – successive refinements.

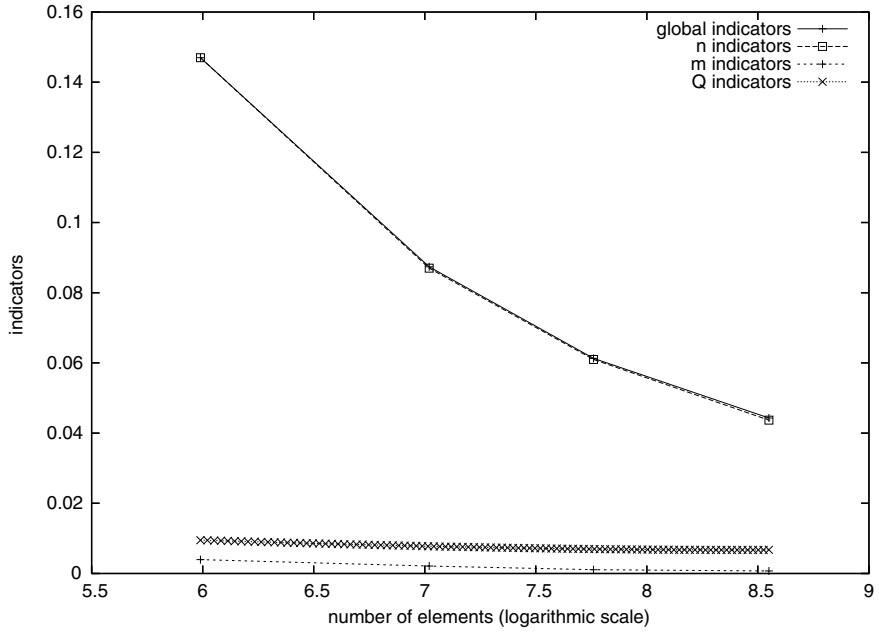

Fig. 41. Cracked cylindrical shell – indicators η, $\eta_n/\sqrt{J_0}$, $\eta_m/\sqrt{J_0}$ and $\eta_q/\sqrt{J_0}$ near the crack tip.

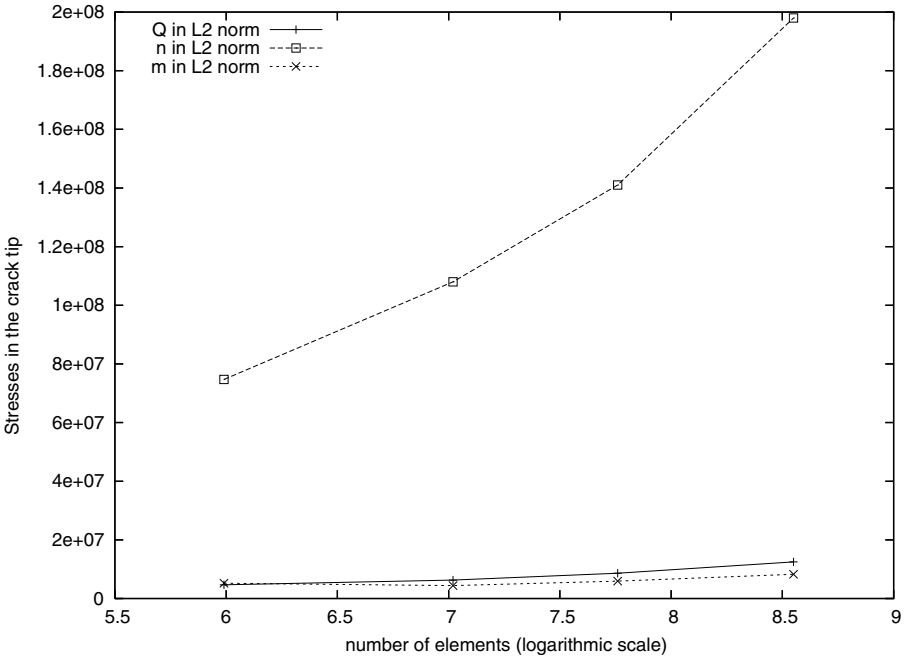

Fig. 42. Cracked cylindrical shell – $\|q\|_{L^2}$, $\|n\|_{L^2}$ and $\|m\|_{L^2}$ near the crack tip.

7. Conclusion

A fundamental problem arising in shell structure approximation, is the geometry. Even if it is known from an analytical expression, it implies a lot of numerical difficulties in the approximation. A first step is to use the definition of a set of vertices displayed on the middle surface of the shell and to assume that the exact normal are known at these points. A consistent numerical scheme can be developed from these reduced informations on the shell geometry [16,20]. But, as in non-linear analysis, when one tries to add new points during a mesh refinement procedure, it becomes necessary to introduce a local approximation of the surface along the edges of each element, in order to define with precision the new points and the new normals at these points. The important feature is that the true informations on the real middle surface of the shell are not necessarily known. Therefore, it has been useful to adapt the strategy introduced in [8] to adaptive mesh refinements. As illustrated on various different shells, we have compared the previous strategy with an exact interpolation of the geometry (the added nodes are on the exact middle surface and the associated normal vectors are also exact). Then, it can be observed that the effect of the geometry interpolation introduced in [8] *on the mesh refinement procedure* is neglectible, and the results obtained in this paper show that the method works with accuracy. Moreover, the introduction, in a more classical local indicator, of the transverse shear forces indicator, as a quantity of interest in the case of shell structures, has been investigated. Its influence can be determinant in the refinement strategy. A further step would be to study more deeply this phenomenon and to introduce other mesh refinement criteria.

References

[1] A. Pica, R.D. Wood, A.O. Adekunle, J. Bonet, Smoothing stress resultants in adaptive finite element shell analysis, Comput. Struct. 54 (5) (1995) 835–849.

[2] T.J. Bond, L.Y. Li, P. Bettess, J.W. Bull, I. Applegarth, Adaptive mesh refinement for shells with modified Ahmad elements, Comput. Struct. 61 (6) (1996) 1135–1141.

[3] C.S. Han, P. Wriggers, An h-adaptive method for elasto-plastic shell problems, Comput. Methods Appl. Mech. Engrg. 189 (2000) 651–671.

[4] R. Lackner, H.A. Mang, Mesh generation and mesh refinement procedures for the analysis of concrete shells, Adv. Engrg. Softw. 33 (2002) 389–402.

[5] M. Cho, S. Jun, *R*-adaptive mesh generation for shell finite element analysis, J. Comput. Phys. 199 (2004) 291–316.

[6] T.J.R. Hughes, J.A. Cottrell, Y. Bazilevs, Isogeometric analysis: CAD, finite elements, NURBS, exact geometry and mesh refinement, Comput. Methods Appl. Mech. Engrg. 194 (2005) 4135–4195.

[7] M. Baumann, K. Schweizerhof, Adaptive mesh generation on arbitrarily curved shell structures, Comput. Struct. 64 (1–4) (1997) 209–220.

[8] I.A. Arregui, M. Salaün, Interpolation d'une surface déterminée par des nœuds et des normales, C.R. Acad. Sci. Paris, Série I 318 (1994) 265–268.

[9] J.Z. Zhu, O.C. Zienkiewicz, The superconvergent patch recovery and a posteriori error estimates. Part 1: The recovery technique, Int. J. Numer. Meth. Engrg. 33 (1992) 1331–1364.

[10] J.Z. Zhu, O.C. Zienkiewicz, The superconvergent patch recovery and a posteriori error estimates. Part 2: Error estimates and adaptivity, Int. J. Numer. Meth. Engrg. 33 (1992) 1365–1382.

[11] F. Cirak, E. Ramm, A posteriori error estimation and adaptivity for linear elasticity using the reciprocal theorem, Comput. Methods Appl. Mech. Engrg. 156 (1998) 51–362.

[12] S. Prudhomme, J.T. Oden, T. Westermann, J. Bass, M.E. Botkin, Practical methods for a posteriori error estimation in engineering applications, Int. J. Numer. Meth. Engrg. 56 (2003) 1193–1224.

[13] M. do Carmo, Differential Geometry of Curves and Surfaces, Prentice-Hall, 1976.

[14] W.T. Koiter, On the foundations of the linear theory of thin elastic shells, Proc. Kon. Ned. Akad. Wetensch B73 (1970) 169–195.

[15] B. Budiansky, J.L. Sanders, On the best first-order linear shell theory, Progr. Appl. Mech., W. Prager Anniversary Volume:129–140, 1967.

[16] Ph. Destuynder, M. Salaün, A mixed finite element for shell model with free edge boundary conditions – Part 1: The mixed variational formulation, Comput. Methods Appl. Mech. Engrg. 120 (1995) 195–217.

[17] P.G. Ciarlet, The Finite Element Methods for Elliptic Problems, North-Holland, 1987.

[18] V. Girault, P.-A. Raviart, Finite element methods for Navier–Stokes equations, in: Theory and Algorithms, Springer Series in Computational Mathematics, vol. 5, Springer, Berlin, 1986.

[19] Ph. Destuynder, M. Salaün, A mixed finite element for shell model with free edge boundary conditions – Part 2: The numerical scheme, Comput. Methods Appl. Mech. Engrg. 120 (1995) 219–242.

[20] Ph. Destuynder, M. Salaün, Approximation of shell geometry for nonlinear analysis, Comput. Methods Appl. Mech. Engrg. 152 (1998) 393–430.

[21] M.C. Rivara, Algorithms for refining triangular grids suitable for adaptive and multigrid techniques, Int. J. Numer. Meth. Engrg. 20 (1984) 745–756.

[22] J.L. Batoz, G. Dhatt, Modélisation des structures par éléments finis – Volume 3: Coques. Hermès, Paris, 1992.

[23] M. Ainsworth, J.T. Oden, A Posteriori Error Estimation in Finite Element Analysis, Wiley, New York, 2000.

[24] Ph. Destuynder, Modélisation des coques minces élastiques, Masson, Paris, 1990.

[25] W. Flügge, Stresses in Shells, second ed., Springer, 1973.

[26] M. Bernadou, Méthodes d'éléments finis pour les problèmes de coques minces, Masson, Paris, 1994.